Investigation of Surface Chemistry, Micro-Topography, and Wettability Alteration of Silica-Asphaltene Interface in Absence and Presence of ZnO and SiO_2 Nanoparticles and a Novel ZnO-SiO_2-Thiazine Nanocomposite using Atomic Force Microscopy and X-Ray Photoelectron Spectroscopy

By:

Togzhan Mynbayeva

Rustem Sherdebayev

Thesis supervisor:

Dr. Ali Shafiei

A thesis submitted to the School of Mining and Geosciences of Nazarbayev University in Partial Fulfillment of the Requirements for the Degree of

Bachelor of Science in Petroleum Engineering

Nazarbayev University

25 April 2023

Acknowledgements

We would like to convey our heartfelt thanks to our supervisor, Dr. Ali Shafiei, for providing us with the chance to conduct research and for his important support throughout the process.

We also like to express our gratitude to our thesis examiner, Dr. Changhong Gao, for his useful feedbacks, which helped us to the improvement of quality of this dissertation.

We also would like to thank Dr. Simin Tazikeh, postdoctoral fellow and research group member, for her kind assistance in various stages of the project especially the experimental part that helped us greatly. We also like to thank Yuliya Ten, Kamilya Arstanova, and Alisher Rakhmetullin from our research team for their help at every stage of the process. We appreciate their guidance and support.

We would like to thank Nazarbayev University for providing financial assistance that allowed us to undertake this study. This research is part of the Collaborative Research Proposal Faculty funding project (091019CRP2103) titled "A comprehensive study on asphaltene characterization and screening asphaltene deposition inhibitors for Kazakhstan crude oils."

Originality Statement

We, Togzhan Mynbayeva and Rustem Sherdebayev, hereby declare that this submission is our work and to the best of our knowledge it contains no materials previously published or written by another person, or substantial proportions of material that have been accepted for the award of any other degree or diploma at Nazarbayev University or any other educational institution, except where due acknowledgment is made in the thesis.

Any contribution made to the research by others, with whom we have worked at NU or elsewhere is explicitly acknowledged in the thesis.

We also declare that the intellectual content of this thesis is the product of our own work, except to the extent that assistance from others in the project's design and conception or style, presentation, and linguistic expression is acknowledged.

Signed on April 25, 2023

Togzhan Mynbayeva _____

Rustem Sherdebayev _____

Abstract

Silica is a primary component of sandstone reservoirs; a very important class of petroleum reservoirs. Presence of asphaltene can modify the surface chemistry of the silica made rocks leading to deleterious effects such as unfavorable wettability condition and deposition of asphaltene. There is insufficient experimental data on changes is silica surface chemistry, micro-topography, and wettability alterations with asphaltene deposition and in absence and presence of nanoparticles (NPs). Therefore, fundamental research is needed to address this research gap. To this end, a thorough experimental research plan was created in three stages: characterization of NPs, preparation of asphaltene deposited silica surfaces, and surface analysis using Atomic Force Microscopy (AFM), Contact Angle (CA) measurements, and X-Ray Photoelectron Spectroscopy (XPS) surveys. Asphaltene was extracted from a Kazakhstani crude oil in accordance with the ASTM D6560-00 standard. The novel ZnO-SiO_2-Thiazine nanocomposite (NC) and its constituent NPs – ZnO and SiO_2 – were characterized using FTIR, TEM, XRD, SEM, and EDX techniques. These techniques were used to determine the size and distribution of NPs, as well as their chemistry, and surface morphology. AFM was used to investigate surface micro-topography of the silica surface samples with asphaltene deposition in presence and absence of NPs/NC. CA measurements were conducted for each sample to assess alteration of wettability in each sample's surface. XPS was used to evaluate elemental composition of the samples to analyze the asphaltene adsorption and its alteration in absence and presence of NPs and NC. XPS Survey has identified C1s, O1s, N1s, S2p, Si2p, and Zn2p orbitals and their atomic ratio present in the samples. Surface images produced by the AFM allowed viewing asphaltene precipitates on a nanoscale and observe the decrease in precipitate quantity in presence of NPs and NC. The CA measurements validated the AFM results by indicating that NPs tend to reduce the CA of the surfaces from oil-wet to intermediate-wet. In contrast, NC has a tendency to decrease the CA from oil-wet to water-wet. High resolution XPS spectra confirmed alterations of the surface chemistry in presence of NPs/NC, and proved that the novel NC to be more effective. The findings of this research work provides more insight into the changes in surface chemistry, micro-topography, and wettability alteration of silica-asphaltene interface in absence and presence of NPs and NC. The findings have significance for design of effective asphaltene precipitation nano-inhibitors and nao-EOR agents.
***Keywords*:** Asphaltene, nanoparticles, silica-asphaltene interface, AFM, XPS, micro-topography, wettability alteration, surface chemistry, asphaltene adsorption.

Nomenclature

Acronyms

AFM	Atomic Force Microscopy
CA	Contact Angle
EDX	Energy Dispersive X-Ray
EOR	Enhanced Oil Recovery
FTIR	Fourier-transform Infrared Spectroscopy
IFT	Interfacial Tension
MS	Mass Spectrometry
NC	Nanocomposite
NP	Nanoparticle
SEM	Scanning Electron Microscopy
TEM	Transmission Electron Microscopy
TRFD	Time-Resolved Fluorescence Depolarization
XPS	X-Ray Photoelectron Spectroscopy
XRD	X-Ray Diffraction

Variables and parameters

S_a	Arithmetical Mean Height, μm
C_{coated}	Atomic concentration of element on asphaltene-coated silica, %
C_{Si}	Atomic concentration of element on silica, %
C_{bulk}	Atomic concentration of element on the bulk asphaltene, %
θ	Contact angle,
θ'	Contact angle for rough surface,
S_{dr}	Developed Interfacial Area Ratio, dimensionless
α	Diffraction angle,
β	Full-width at half maximum of diffraction peak, rad
σ_{lv}	IFT of liquid-vapor interaction, mN/m
σ_{sl}	IFT of solid-liquid interaction, mN/m
σ_{sv}	IFT of solid-vapor interaction, mN/m

S_{ku}	Kurtosis, dimensionless
S_p	Maximum Peak Height, μm
S_v	Minimum Valley Height, μm
D	Particle Size, nm
S_q	Root Mean Square Height, μm
r	Roughness factor, dimensionless
k	Scherer's constant (k=0.94), dimensionless
S_{sk}	Skewness, dimensionless
f	Wetted solid surface area fraction, dimensionless
λ	X-ray wavelength, nm
S_y	Z Value Range, μm

List of Figures

List of Tables

1 Introduction

This chapter begins with a definition of asphaltene, its characteristics, and processes related with it such as aggregation, precipitation, and deposition. Following that, a brief explanation of present asphaltene deposition techniques is provided, as well as the reasons behind their inefficiency. The problem statement is formed, followed by the recommended research objectives and methodology. This chapter also concludes a description of the research work's organization and structure.

1.1 Background

Upstream oil production is quite a dynamic process that leads to considerable alterations in temperature, pressure, and oil composition in a reservoir. Variations in these key parameters in reservoirs with high asphaltene content lead to detrimental consequences – precipitation/deposition of asphaltene, a highly heavy and complex component of crude oil, at any place and stage of the oil production which includes porous media, well columns, production units, refineries, and subsurface transportation pipelines (Zendehboudi, 2019). The aforementioned consequences of asphaltene precipitation in a porous media result in severe alterations in reservoir rock properties such as permeability reduction and wettability alteration accompanied by increased oil viscosity which eventually reduces oil production (Zendehboudi, 2019). Moreover, along with the reduction in oil production, there are other financial problems like equipment damage and unpredicted use of capital and operating expenditures of a company to treat the consequences of asphaltene deposition (Zendehboudi, 2019). Therefore, asphaltene deposition is one of the significant issues of the petroleum industry; however, it has not been overcome yet. In order to conduct comprehensive research, it is necessary to give a clear definition of some terms.

Asphaltenes are classified as a solubility class due to their sophisticated chemical composition and structure. These compounds are made of hydrogen and carbon with a H/C atomic ratio ranging from 0.8 to 1.4; as well as some heteroatoms and metals such as nitrogen, oxygen, sulfur, iron, vanadium, and nickel, respectively (Zendehboudi, 2019; Tazikeh, et al., 2021). ***Aggregation*** is the generic growth process of asphaltene molecules from nanometer to micrometer scale. ***Precipitation*** is the process of transforming from stable to micrometer-sized asphaltene aggregates (Alian, et al., 2011). ***Asphaltene deposition*** is the process of asphaltene aggregates attaching onto a surface (Hoepfner, et al., 2013).

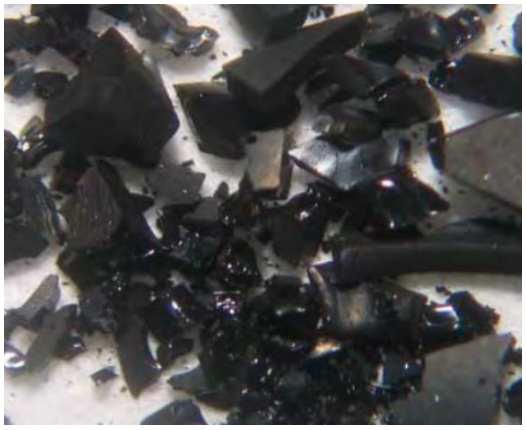

Figure 1-1. Separated asphaltene using toluene *(Abdel-Raouf, 2012)*

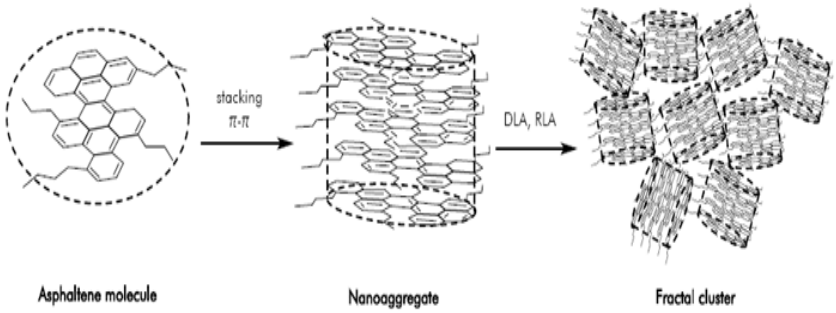

Figure 1-2. Asphaltene aggregation *(Morante, et al., 2017)*

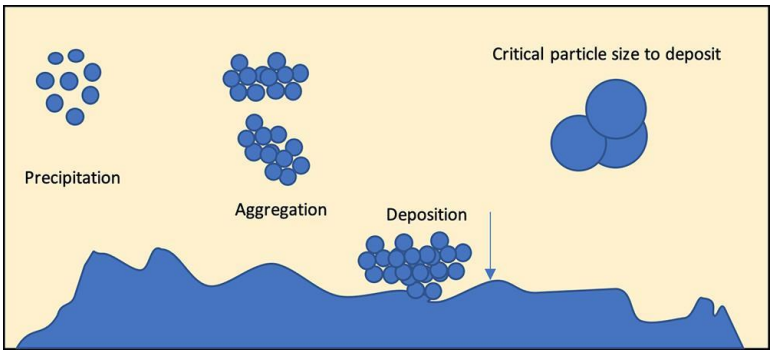

Figure 1-3. Asphaltene aggregation and deposition *(Al-Hosani, et al., 2021)*

There are numerous factors affecting asphaltene deposition. One of them is the chemical composition of crude oil. In highly stable oils asphaltene molecules have low aromaticity and high hydrogen content. In unstable crude oils, the trend is the opposite (Keshavarz, et al., 2019). Another factor is the water content in the reservoir, as water content increases, asphaltene precipitation and deposition become more complex. The reason for this is that formation water

contains ions, which interact with asphaltene and prohibit its aggregation (Hu, et al., 2015). Also, thermodynamic factors such as pressure and temperature affect asphaltene deposition. Asphaltene precipitation starts below the bubble point, below which gas evaporates from the oil mixture, and oil becomes heavier. In this heavy oil asphaltene solubility increases, therefore the precipitation decreases (Hirschberg, et al., 1984; Vargas, et al., 2009). The temperature effect shows that as temperature rises, asphaltene precipitation decreases (Afshari, et al., 2010). The last factor affecting asphaltene deposition is an electro-kinetic effect. The electro-kinetic effect states that the flow of fluids inside the reservoir pores and tubing generates electrical potential which destabilizes the stability of asphaltene molecules. As the fluid velocity rises, the precipitation increases (Kokal & Sayegh, 1995; Sarma, 2003).

To date, in the petroleum industry, there are some existing treatment methods applied to solve asphaltene deposition problems such as thermal, mechanical, chemical, ultrasonic, and bacteria treatments. ***Thermal treatment*** includes hot oiling, a down-hole heater, and heat-liberating chemicals. Each of these thermal treatment techniques has its own drawback (Bruining, et al., 1990). Down-hole heaters need high quantities of electric energy, therefore this method is highly expensive. Injection of hot oil may cause formation damage, therefore it is not widely acceptable (Bernadiner, 1993). The last one is heat-liberating chemicals, which are presented as an equimolar mixture of sodium nitrate and ammonium chloride. Additionally, the high cost of this method restricts it to be widely used in the industry. ***Mechanical treatment*** is based on the mechanical scraping of asphaltene deposits inside the well. It includes a wireline unit, however, it is expensive and slow in long and hard asphaltene deposits. The second alternative to mechanical treatment is hydro-blasting tools. However, the limitation of this tool is low working pressure (Akbar & Saleh, 1989). ***The chemical treatment*** technique is based on the aromatic nature of asphaltene that requires using aromatic solvents to dissolve asphaltene deposits. The most common asphaltene solvent is xylene. The chemical treatment has its own disadvantages such as the risk of safety and corrosion of the equipment. To mitigate asphaltene precipitation nonionic surfactants such as ethoxylated alcohols/phenols, their high efficiency is explained due to the significant interaction with asphaltene (Ramos, et al., 2001). ***The ultrasonic treatment*** utilizes ultrasonic waves that propagate through the asphaltene structure and break the continuous phase of asphaltene. The efficiency of this method is tested for carbonate reservoirs, where ultrasonic waves decompose asphaltene deposits into fine-sized grains and improve reservoir permeability

(Gollapudi, et al., 1994). ***Bacteria treatment*** is an efficient injection method due to bacteria's stability in high temperature and salinity conditions and effectiveness in permeability improvement (Almehaideb & Zekri, 2001).

1.2 Statement of problem

The research addresses the problem of asphaltene deposition that hinders oil production by deteriorating both production facilities and reservoir rock properties (Zendehboudi, 2019). These repercussions may range from equipment replacement to well abandonment, with costs ranging from $70 million to $150 million (Vargas & Tavakkoli, 2018). The issue of asphaltene deposition is international in scope. In fact, even reservoirs with the lowest asphaltene content can experience significant deposition, as happened in Algeria's Hassi Messaoud oil field in 1965, which had only 0.06 wt% asphaltene (Vargas & Tavakkoli, 2018).

Since the last century, various asphaltene deposition treatment methods were investigated, though each has its own set of restrictions and degree of efficiency. Nanoparticles are now a hot issue in several scientific domains, including the petroleum sector. Because of their ability to adsorb onto asphaltene molecules, nanoparticles have been shown to be effective asphaltene inhibitors (Sun, et al., 2017). Their great efficiency can be attributed to their tiny size (1-100 nm), which allows them to flow through narrow pores and cover a reasonable surface area, hence boosting oil recovery.

The primary research question that our thesis will address is the efficacy of ZnO-SiO_2-Thiazine nanocomposite as an asphaltene inhibitor compared to its constitute nanoparticles – ZnO and SiO_2. The research addresses the issue of insufficient experimental data on silica surface topography, wettability, and surface chemistry alterations with asphaltene deposition in absence/presence of NP/NC.

1.3 Research objectives

This Capstone Project aims to investigate the effectiveness of ZnO-SiO_2-Thiazine NC and its constituent NPs separately as asphaltene inhibitors on silica surface. The main research objectives of the Capstone Project are:

- To investigate the effect of NC and NPs on asphaltene precipitation by measuring the surface roughness of silica surface.
- To investigate the effect of NC and NPs on wettability alteration by measuring the contact angle of silica surface.

- To investigate the effect of NC and NPs on asphaltene adsorption on silica surface.
- Additional aim is to demonstrate usage of NC and NPs as potential EOR-agents.

This research results can be used for the development of more effective asphaltene inhibitors, particularly for reservoir rocks consisting of silica (i.e. sandstone).

1.4 Research methodology

This is an experimental study carried out Core Facilities of Nazarbayev University, and laboratories of SMG and Dr. Ali Shafiei. Chapter 3 describes in full each experiment, the materials involved, and the sample preparation procedure. The methodology of the study consists of 5 parts:

1. Extraction and characterization of asphaltene from Kazakhstani crude oil using XPS;
2. Characterization of NC and NPs based on FTIR, TEM, XRD, SEM, and EDX techniques which assess particle's size and distribution, chemical analysis, and surface morphology;
3. Preparation of silica surface samples with separate procedures for XPS and AFM. The samples prepared were: silica + asphaltene + n-heptane, silica + asphaltene + n-heptane + ZnO, silica + asphaltene + n-heptane + SiO_2, and silica + asphaltene + n-heptane + NC;
4. Conduction of AFM and CA measurements in ambient conditions on each prepared silica surface sample, including pure silica;
5. Conduction of XPS Survey on each prepared silica surface sample, including pure silica. Identification of C1s, O1s, N1s, S2p, Si2p, and Zn2p orbitals on surface samples based on XPS overall survey and interpretation of high-resolution XPS spectra for each identified orbitals.

1.5 Thesis structure

The report consists of five chapters. Chapter 2 is the literature review where nature of asphaltene and how it aggregates and precipitates, the factors affecting the asphaltene adsorption to occur, the nature of NPs, the mechanism of asphaltene inhibition by NPs and behavior of different reservoir rock surfaces in presence asphaltene and NPs are described. Chapter 3 is the Materials and Methods where silica surface, asphaltene and NPs/NC, sample preparation methods, and the techniques used to assess the efficiency of NPs/NC are described. The research findings including NPs/NC characterization, AFM, XPS, and CA measurements are discussed in Chapter 4 followed by conclusions and recommendations for further research presented in Chapter 5.

2 Literature Review

In this section, the asphaltene definition and its properties are discussed. The discussion is followed by description of mechanisms of asphaltene aggregation and adsorption as well as the variables that influence these processes. Furthermore, nanoparticles and the mechanisms by which they inhibit asphaltene are introduced, along with their role as EOR agents. This chapter is concluded with references to pertinent research on the effects of asphaltene precipitation and deposition on wettability, surface morphology and micro-topography of rock surfaces.

2.1 Chemical composition and structure of asphaltene

Asphaltene is organic compound that is mainly made of carbon-hydrogen bonds, also heteroatoms like N, O, S, and trace metals of transitional (Rodgers & Marshall, 2007). Asphaltene is a polar chemical compound with varying molecular weight. The molecular weight of asphaltene varies because of the aggregation of asphaltene molecules which prohibit measuring actual asphaltene molecular mass. From Time-Resolved Fluorescence Depolarization (TRFD) and Mass Spectrometry (MS) measurements the common asphaltene's molecular weight ranges from 250 to 1200 g/mol, and the mean is 750 g/mol (Andrews, et al., 2006; Groenzin & Mullins, 1999; Poveda, et al., 2014). The average asphaltene molecule has the following approximate mass fractions of heteroatoms and metals: sulfur (7 %), oxygen (1.5 %), nitrogen (1.1 %), vanadium (700 ppm), and nickel (200 ppm). The approximate molecular formula of the asphaltene molecules with 3000 g/mol molecular weight is presented as $C_{205}H_{236}S_7O_3N_2$ (Wiehe, 2012).

Although the molecular mass of asphaltene is well understood, the discussion about the chemical structure of asphaltene is active. There are two major chemical structures of asphaltene: island and archipelago. Island structure was discovered by Yen and his co-workers in the 1960s using X-ray diffraction. In island structure asphaltene's aromatic cores are sharing the common carbon bonds and condensed into one big core composed of 7-15 fused rings (Mullins, 2010), which is surrounded by alkyl chains and polar functional groups, containing heteroatoms. The example of Island structure is presented in Figure 2-1.

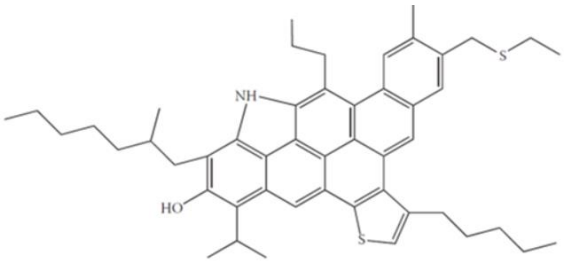

Figure 2-1. Example of asphaltene island structure (Hasanvand, et al., 2018)

Island structure has some drawbacks which refute this concept, for example island structure is inconsistent with upgraded products from crude oil asphaltene. Furthermore, island structure cannot explain abundant anthracene, benzene, and naphthalene derivatives from thermally applied asphaltene (Strausz, et al., 1992; Rueda-Velasquez, et al., 2013; Karimi, et al., 2011). The alternative asphaltene structure is the archipelago. The structure is based on interconnected asphaltene rings using carbon chains (Sheremata, et al., 2004; Podgorski, et al., 2013). One of the possible asphaltene archipelago structure is shown in Figure 2-2.

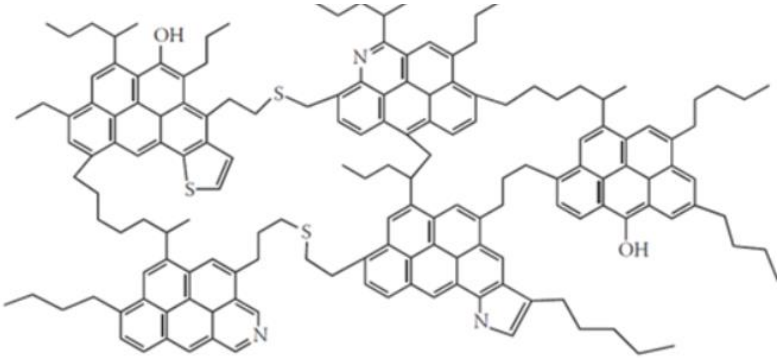

Figure 2-2. Example of asphaltene archipelago structure (Hasanvand, et al., 2018)

2.2 Asphaltene aggregation

Asphaltene problem arises due to the aggregation of asphaltene molecules and the consequent precipitation and deposition. Asphaltene aggregation is the process of attachment of numerous asphaltene molecules to each other, which lead to the formation of a cluster. The process of aggregation starts from crosslinking of separate asphaltene molecules and formation of nanoaggregates. After this, asphaltene nanoaggregates with concentration of 50-100 mg/L are forming into clusters with the size between 3-10 nm. The size of molecules is determined using X-ray and SANS techniques (Dickie & Yen, 1967).

The aggregation process of island structure asphaltenes is explained by π-stacking of asphaltene's aromatic rings. This mechanism of aggregation was proposed in the early 2000s using fluorescence depolarization (Groenzin & Mullins, 1999; Buenrostro-Gonzalez, et al., 2001) and molecular imaging (Schuler, et al., 2015).

There are different popular asphaltene aggregation models. One of them is the Yen model, where the asphaltene micelle has a core structure surrounded by the resin molecules. The illustration of different stages of asphaltene aggregation is presented in Figure 2-3.

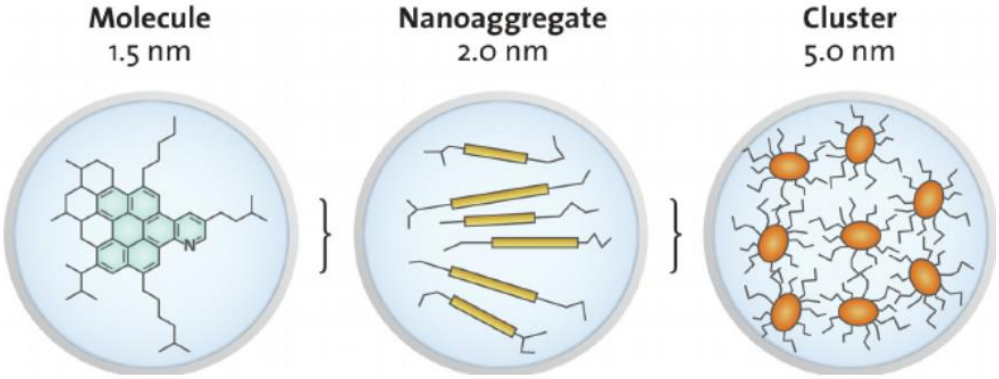

Figure 2-3. Asphaltene aggregation based on Yen model (Seifert, et al., 2012)

The micelle sizes are 1.6 – 2.0 nm in high and 0.8 – 1.6 nm in wide (Dickie & Yen, 1967). Yen-Mullins model of asphaltene aggregation starts from formation of nanoaggregates with asphaltene molecules of island structure. The aggregation number is approximately six. After these nanoaggregates are forming clusters with the aggregation number of eight (Acevedo, et al., 1997). The next model is the compatibility model by Wiehe (2012). The aggregation principle of this model is based on dynamic equilibrium. In the oil mixture asphaltene molecules are dispersed by resins. Asphaltene – resin association shift from the equilibrium may happen due to the decrease of resin and/or asphaltene content or increase of saturates (Wiehe, 2012).

2.3 Factors affecting the asphaltene adsorption

In this research paper asphaltene adsorption plays a key role. There are different factors affecting asphaltene adsorption on the surface. One of them is the surface type. Asphaltene molecules commonly are strongly adsorbed to solid surfaces, which are presented commonly as silica, kaolin, dolomite, and metals. Minerals are considered as the most reactive material for asphaltene adsorption (Jada & Debih, 2009). The most common minerals which are used for adsorption

studies are dolomite, quartz, feldspar, calcite, hematite, limestone, fluorite, and sandstone. The adsorption efficiency experiment's results showed the next sequence from the most reactive asphaltene adsorption to the least reactive one: kaolinite > calcite > quartz > dolomite. Thus, kaolinite has the highest adsorption reactivity, whereas dolomite has the lowest adsorption reactivity from the studied minerals (Mohammadi, et al., 2012).

Another factor is the chemical composition of asphaltene molecules. If asphaltene contains a high number of heteroatoms such as N, O, then the asphaltene adsorption efficiency increases. It was found that the content of heteroatoms in the asphaltene has more impact on asphaltene adsorption efficiency than the overall composition of the molecule. The adsorption experiments carried on the Athabasca bitumen showed that N and O heteroatoms have an important impact on the adsorption process, while sulfur is not important due to the formation of weaker dipoles (González, et al., 2007; López-Linares, et al., 2006).

In addition, solvent type crucially affects the asphaltene adsorption. If the reservoir contains water, then in aqueous and dielectric organic solvents the main mechanism is ion exchange, while in less polar organic solvents the dominant forces are acid-base coordination, van der Waals, and H-bonding.

The chemical composition of crude oil has a significant impact on asphaltene adsorption. For example, resins' content in crude oil may increase or decrease asphaltene adsorption efficiency according to different research. According to Ekholm et al. (2002), the thickness of adsorbed asphaltene increases when resins and asphaltenes are present in asphaltene. The main reason for this is the swelling of the aggregates from intercalation of resins into the aggregates (León, et al., 2002).

In addition, physical size of asphaltene molecules and asphaltene aggregates affect the adsorption. The reason for the effect of physical size of asphaltene on its adsorption is explained by dependence of sorbent's active sites and surface area of asphaltene's active sites. As asphaltene becomes bigger it has higher surface area, as a result they have high probability of buried functional groups, and consequently more likely to react with sorbent active sites (Abudu & Goual, 2009).

The temperature effect on asphaltene adsorption was studied by Pierre et al., who concluded that as temperature rises the amount of adsorbed asphaltene molecules decreases (Pierre, et al., 2004). However, there are a few exceptions. Firstly, at 250°C some asphaltene

molecules are aggregated into two size regimes: large diameter and small diameter distributions relative to the normal size at 150°C (Acevedo, et al., 2012). Thus, smaller aggregates.

2.4 Nanoparticles as asphaltene inhibitors

Though the asphaltene adsorption on a reservoir rock surface reduces the amount of asphaltene content in crude oil and has negligible effect on rock porosity, it does affect permeability and wettability of reservoir rock in an unfavorable manner (Zendehboudi, 2019). Therefore, it is essential to be able to remove asphaltene precipitates or at least delay its onset point. There are various asphaltene deposition treatment methods discussed in the introductory part, however the application of nanoparticles in the petroleum industry is one of the modern research interests due to its high efficiency, environmental friendliness, and cost-effectiveness (Sun, et al., 2017).

NPs are described as metal oxide particles (e.g., MgO, NiO, SiO_2, Al_2O_3) with a size in the range of 1-100 nm (Sun, et al., 2017). The Scanning Electron Microscopy (SEM) image of γ-Al2O3 nanoparticle is presented in Figure 2-4. NPs possess inhibiting properties by postponing the onset point of asphaltene precipitation which is executed in 2 ways: 1) elimination of asphaltene from the crude oil, and 2) bond formation between NPs and asphaltene molecules (Shojaati, et al., 2017).

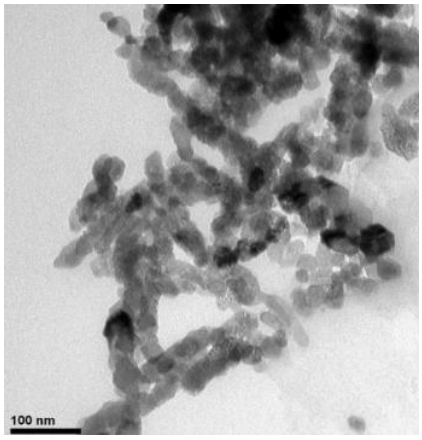

Figure 2-4. SEM of γ-Al_2O_3 NPs (Shojaati, et al., 2017)

The asphaltene elimination is realized by the adsorption of asphaltene molecules (adsorbates) onto the surface of NPs (adsorbents), thus removing the asphaltene molecules from the oil system (Sun, et al., 2017; Shojaati, et al., 2017) as shown in Figure 2-5. The asphaltene removal is considered to be an inhibiting factor due to the fact that the less the asphaltene

concentration in the oil, the less there is the probability of asphaltene precipitation/deposition (Shojaati, et al., 2017).

The second way of onset delay is closely linked to the asphaltene adsorption onto the NPs' surface discussed above. In fact, it was investigated that the process of asphaltene adsorption is essentially a polar interaction (Shojaati, et al., 2017; Nassar, et al., 2011). Based on the conducted studies, it was revealed that NPs with acidic nature tend to adsorb asphaltene better than amphoteric ones, due to the formation of stronger polar bonds, thus leading to the conclusion that asphaltene molecules are basic in nature (Shojaati, et al., 2017; Nassar, et al., 2011). The formation of polar bonds makes asphaltene molecules be suspended in the fluid, like resins, therefore delaying the onset of precipitation (Shojaati, et al., 2017). Even though this delay is an interim solution, it still gives impetus to increased oil production, since the presence of NPs in the oil system stabilizes the remaining asphaltene molecules, thus decreasing the probability of their deposition (Shojaati, et al., 2017).

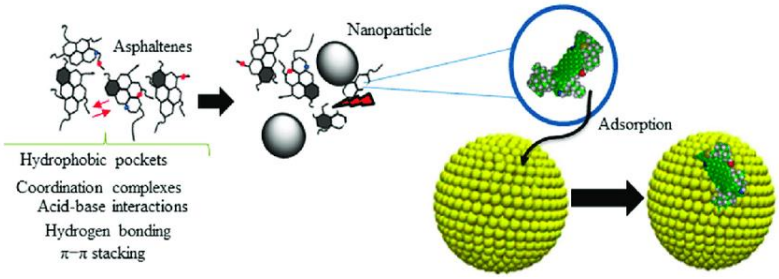

Figure 2-5. Asphaltene adsorption mechanism of nanoparticles (Medina, et al., 2019)

2.5 Selection of NPs based on their chemical nature

Since there is a wide range of metal oxides, it is necessary to determine which of them are more efficient in use. As it was discussed, due to polar interactions occurring between asphaltene (base) and NPs (acid), metal oxides with acidic nature are preferable. According to the study conducted by Shojaati et al. (2017), it was discovered that 2 acidic NPs do not have the same adsorbing efficiencies. Such phenomenon is explained by the fact that the real determinant of adsorption efficiency is not only the adsorbent's chemical nature but the type of its constitutive acid. The interaction of adsorbate with Bronsted acid was revealed to be more polar than with Lewis acid, hence Bronsted acid metal oxides are more preferred in industrial use. Additionally, the highest onset point delay (i.e. the strongest adsorption) was observed for the NPs that form hydrogen bonding with asphaltene molecules.

2.6 Nanoparticles as EOR agents

As the world develops on a daily basis, so does the need for oil and gas, which is getting increasingly difficult to extract. As a result, researchers are concentrating their efforts on developing ways for recovering non-producible petroleum. The developing petroleum industry sector - EOR - is also very interested in the application of nanotechnology. The grounds for this intense attention are as follows: 1) great stability of NPs; 2) ease of modifying NPs physical and chemical characteristics; and 3) environmental friendliness (Agista, et al., 2018). Figure 2-6 depicts the EOR effect of NP: in the absence of NP, water flooding was unable to recover trapped oil (brown-coloured), however with the addition of the nanoparticles, more crude oil was retrieved, including the previously trapped oil bank (Li, et al., 2021).

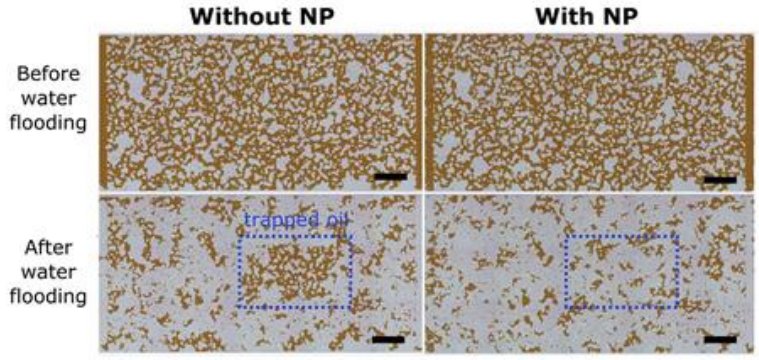

Figure 2-6. NP effect on water flooding efficiency (Li, et al., 2021)

The mechanisms governing the EOR ability of NPs are IFT reduction, wettability alteration, viscosity control, and disjoining pressure (Agista, et al., 2018). Throughout the porous media, these mechanisms arise as NPs adsorb, desorb, and transport due to the van der Waals forces, Born repulsion, acid-base interaction, hydrodynamic energy, and electric double-layer repulsion (Agista, et al., 2018). The study conducted by Kumar, et al. (2022) has investigated the effect of disjoining pressure mechanism on oil-saturated sandstone using Silica nanofluid, as displayed in Figure 2-7. The Figure depicts the sandstone core immersed in nanofluid. On a smaller scale, the oil droplet has wedge-shaped film due to electrostatic repulsion and Brownian motion, resulting in a disjoining pressure gradient. The disjoining pressure is raised due to presence of positively charges silica NPs. As a result, the oil droplet is separated from the sandstone surface, boosting oil recovery.

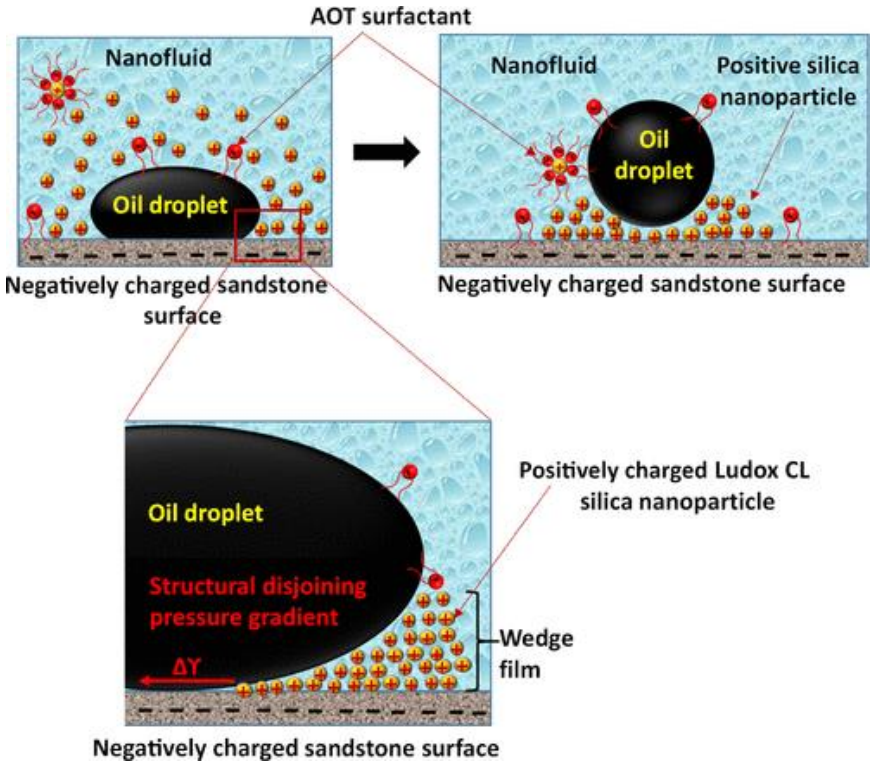

Figure 2-7. Oil imbibition caused by disjoining pressure mechanism (Kumar, et al., 2022)

The most commonly used material in EOR activities is silica NP (SiO_2), which is used both for its versatility in operating as a hydrophobic and a hydrophilic material as well as for its simplicity of manufacture. Hendraningrat et al. (2013) conducted a research that found that while silica NP concentration increases reduce contact angle, excessive concentrations (>0.1 wt%) may cause pore blockage. Thus, the reasonable NP concentration should be selected.

Zinc Oxide, one of the widely used NP, is renowned for altering surface wettability and reducing the viscosity of heavy oils. The study proved that ZnO NP is significantly more efficient on sandstone than carbonate, as 0.2 wt% of ZnO NP increased oil recovery of sandstone by 20.68% OOIP, whilst for carbonate only by 8.89% OOIP (Tajmiri, et al., 2015).

2.7 The asphaltene adsorption on reservoir rocks

Due to the focus of the study, it is significant to examine different rock surfaces and their interactions with asphaltene. According to the aforementioned study, it is known that kaolinite and calcite minerals are more feasible to be adsorbed by asphaltene, whereas quartz and dolomite are less feasible for adsorption (Jada & Debih, 2009; Mohammadi, et al., 2012).

The key parameter used to evaluate the interaction of a rock surface with asphaltene

adsorption in the presence/absence of NPs is the wettability of a rock surface. As it was mentioned, asphaltene adsorption causes the wettability of the rock surface to change and there are different perspectives on types of causes of wettability alteration occurring due to the adsorption. According to one study, the wettability alteration occurs due to the following factors: brine/oil composition, rock chemistry, and rock−fluid interactions (Mohammed, et al., 2021). The impact of the aforementioned factors varies in different rocks, thus it is more challenging to make a general trend on asphaltene adsorption on various rock surfaces, instead, and each mineral must be considered separately. According to the other study, asphaltene precipitation alters the surface properties of a reservoir rock by making it more heterogeneous (Tazikeh, et al., 2022). This effect is observed with the help of the roughness height parameter – the larger the roughness height, the larger becomes the contact angle too (Tazikeh, et al., 2022). Therefore, the change in contact angle leads to alterations in wettability, where a rock surface gets strongly oil-wet. According to the study, the presence of NPs in the oil system prevents alterations in the roughness height, thus preventing the wettability changes, i.e. the wettability of a rock surface shifts from strongly oil-wet to preferentially oil-wet or even water-wet (Tazikeh, et al., 2022; Eltoum, et al., 2021).

2.8 Surface analysis and wettability measurements

2.8.1 Surface roughness

Surface roughness has significant importance in wettability alteration of petroleum reservoirs, which affects the production of the oil and gas. There are numerous research which focused on investigating surface morphology. One of the methods which can be used to assess surface morphology is AFM (Atomic Force Microscopy). AFM is able to get sufficient two-, three-dimensional images of a surface in addition to quantitative surface topography parameters in the x, y, z - space directions (Tazikeh, et al., 2022). The surface topography parameters with their description and corresponding formula are summarized in Table 2-1.

Table 2-1. Statistical parameters for roughness (Tazikeh, et al., 2020; 2022)

Parameter	Description	Formula
Maximum Peak Height S_p	This parameter defines the height of the highest peak of an examined area	-
Minimum Valley Heights S_v	This parameter defines the height of the lowest valley of an examined area	-
Arithmetical Mean Height S_a	An absolute number that reflects the difference in heights between each point	$S_a = \iint_a \lvert Z(x,y)dxdy \rvert$
Z Value Range S_y	The difference between the highest and the lowest points of an examined area	$S_y = S_p - S_v$
Root Mean Square Height S_q	The standard deviation of heights from the mean value	$S_q = \sqrt{\iint_a (Z(x,y)^2 dxdy}$
Skewness S_{sk}	Skewness describes the symmetry of height distribution. If the skewness is zero, the height distribution is symmetrical. Positive skewness results in high peaks and shallow valleys, whereas negative skewness results in no peaks but deep stretches	$S_{sk} = \frac{1}{S_q^3}\left[\frac{1}{\mathrm{A}}\iint_A Z^3(x,y)dxdy\right]$

Kurtosis S_{ku}	The kurtosis parameter describes the peak form. The greater the value, the sharper and closer the peaks are to each other.	$S_{ku} = \frac{1}{S_q^4}\left[\frac{1}{A}\iint_A Z^4(x,y)dxdy\right]$
Developed Interfacial Area Ratio S_{dr}	This value is a percentage that represents the additional surface area that the texture provides over a perfect plane. S_{dr} is influenced by both the texture amplitude and spacing. As a result, a texture with a higher S_a and wider spacing can have a lower S_{dr} value than a texture with a lower S_a but tighter spacing.	$S_{dr} = \frac{\iint_A \left(\sqrt{\left[1+\left(\frac{\partial z(x,y)}{\partial x}\right)^2+\left(\frac{\partial z(x,y)}{\partial y}\right)^2-1\right]}\right)dxdy}{A}$

2.8.2 Wettability measurement

As previously discussed, asphaltene adsorption onto a reservoir rock surface leads to changes in its wettability. The wettability alteration of a reservoir rock is commonly indicated by the corresponding alterations in the contact angle and measuring it is acknowledged to be one of the simplest and most practical methods (Kumar, et al., 2004). Contact angle characterizes the point at which oil and water interface meet at the rock surface; thus the contact angle method measures the shift in rock surface affinity of one fluid to another (Mohammed & Babadagli, 2015).

According to the Young equation, contact angle is a function of Interfacial Tension (IFT) between 3 phases – solid, liquid, and vapor – and is described by the following equation (Nakajima, 2011):

$$\cos\theta = \frac{\sigma_{sv} - \sigma_{sl}}{\sigma_{lv}}$$

From the Young equation, it can be seen that surface roughness is not considered in the calculations, however, this factor is the important one. Since reservoir rock is porous, thus its surface heterogeneity may vary, in order to get the most accurate and reliable results the effect of roughness must be taken into consideration (Mohammed & Babadagli, 2015). Therefore, Wenzel

has revised the Young Equation by taking into consideration a roughness factor r and thus contact angle for rough surface θ' (Nakajima, 2011):

$$\cos\theta' = r\left(\frac{\sigma_{sv} - \sigma_{sl}}{\sigma_{lv}}\right) = r\cos\theta$$

Additionally, some rock surfaces may have too high roughness factor such that vapor invades between the solid and liquid, thus complicating the contact angle measurement. For such cases, Cassie has developed an equation based on the Young and Wenzel equations by introducing a new parameter – a wetted solid surface area fraction f (Mohammed & Babadagli, 2015):

$$\cos\theta' = f\cos\theta + f - 1$$

The rock wettability can be classified based on the obtained contact angle values, where $\theta < 75°$ represents the water-wet surface, $75° < \theta < 105°$ is for the intermediate-wet, and $\theta > 105°$ for the oil-wet (Kaveh, et al., 2014).

3 Materials and Methods

A substantial portion of this study is based on laboratory experiments that examine asphaltene precipitation/adsorption events on silica surfaces from multiple perspectives. The first stage is to prepare the necessary materials, which includes the synthesis of the nanocomposite utilized, the extraction of asphaltene from crude oil, and the manufacture of synthetic oil, which is required for sample surface preparation. Following that, the physical and chemical properties of the materials to be employed must be determined. The extracted asphaltene is characterized using XPS, whilst the NPs/NC are characterized using FTIR, TEM, SEM, EDX, and XRD in addition to the aforementioned approach. Following that, silica sample surfaces are created under two distinct circumstances. The first condition is used to explore the influence of NPs/NC on *asphaltene precipitation* on a silica surface as measured by AFM and CA. The second condition is added to explore the influence of NPs/NC presence on *asphaltene adsorption*, which is then analyzed using XPS. The technique flowchart shown in Figure 3-1 schematically depicts all laboratory methods covered in this chapter.

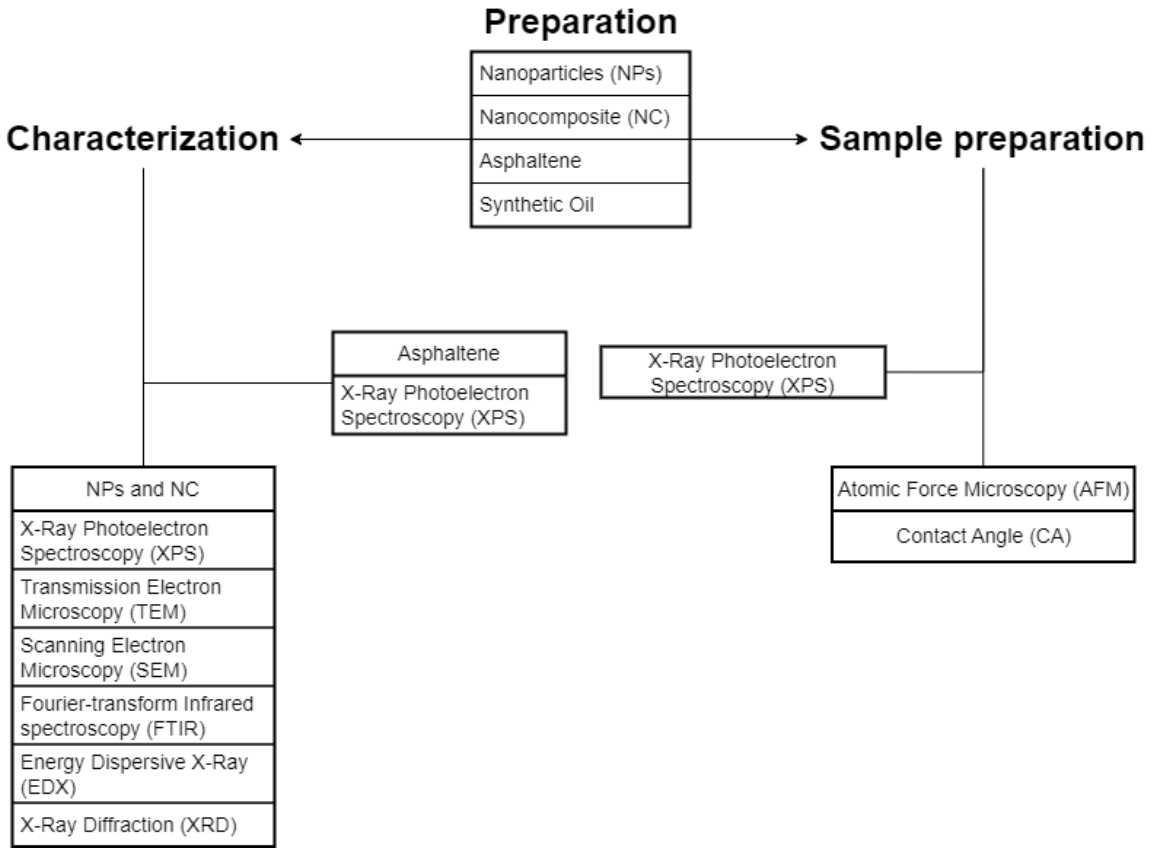

Figure 3-1. Methodology flowchart.

3.1 Materials

The materials used for preparing samples include metal NPs – silicon dioxide (SiO_2) and zinc oxide (ZnO), and nanocomposite ZnO-SiO_2-Thiazine made of these NPs. NC preparation requires dried powdered leaves of the *Centella asiatica L*, $ZnCl_2$, Na_2SiO_3, Thiazine, and Na_2CO_3. The asphaltene was extracted from the crude oil of West Kazakhstan oilfield. *n*-heptane and toluene are used as solvents to extract and purify the asphaltene. The surface material for asphaltene precipitation (adsorbent) was a silica surface.

3.2 Preparation of the nanocomposite

ZnO-SiO_2-Thiazine nanocomposite preparation is based on the extract of *Centella asiatica L*. To obtain the plant extract, 50 grams of its dried powdered leaf is boiled in double distilled water of 400 ml at 80°C for 40 minutes. Afterward, the extract is filtered, cooled, and stored in the refrigerator. The next step is the preparation of the NC itself and its mechanism is presented in Figure 3-2. To prepare the NC, 2 g of $ZnCl_2$, 4 g of Na_2SiO_3, and 6 g of Thiazine (for functionalization) are added to 100 mL of the *Centella asiatica L* plant extract in a 250 ml flask. The flask's content is refluxed by keeping the basic conditions of pH = 9 (adjusted by the addition of 0.1 M Na_2CO_3) and stirred at 60ºC for 24 hours until the complete formation of the NC. Finally, the mixture is filtered and the left precipitate is dried and kept for further characterization and sample preparation purposes.

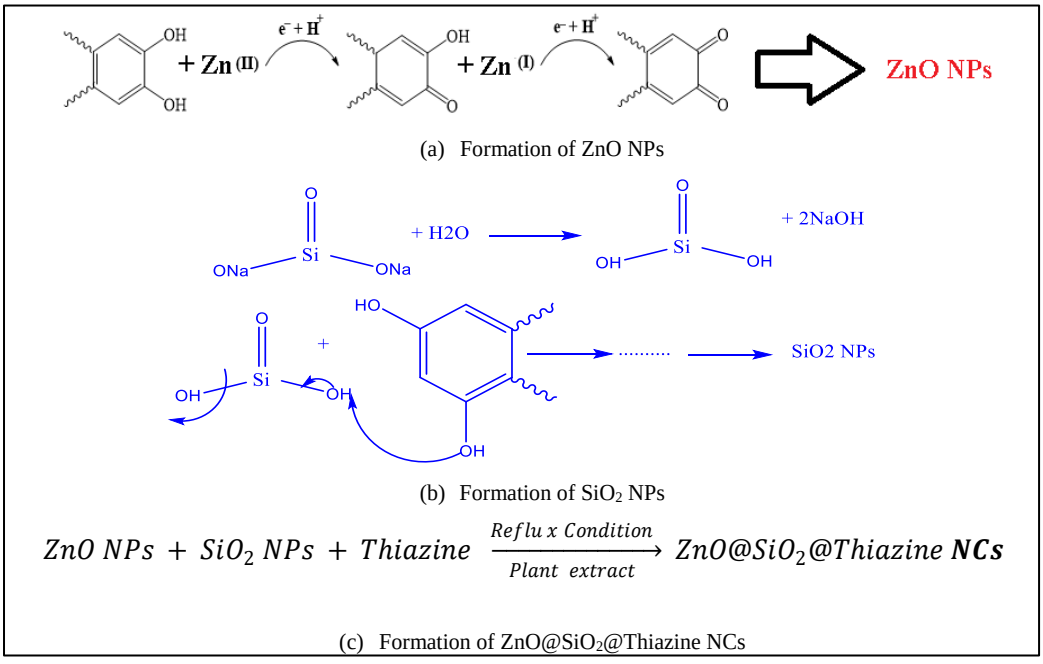

Figure 3-2. The mechanism proposed for biosynthesis of the NC.

3.3 Asphaltene extraction

In this study, the standard asphaltene extraction procedure ASTM D6560-00 is applied (American Society for Testing and Material, 2013) and its scheme is presented on Figure 3-3. Initially, the mixture of the crude oil with *n*-heptane is obtained by mixing them with a volumetric ratio of 1:40 with a duration of 4 hours. The mixture is a precipitate which is centrifuged to eliminate the solid phase from it. The next step is to create a mixture by adding 30 ml of n-heptane to each 1 g of the extracted solid phase. The mixture is put under the reflux for an hour followed by placing the obtained solution in a dark place for 150 minutes to remove and dissolve the wax present in the created mixture. Afterward, the precipitated asphaltene is filtrated from the solution with the help of Whatman No. 42 filter paper positioned as shown in Figure 3-4.

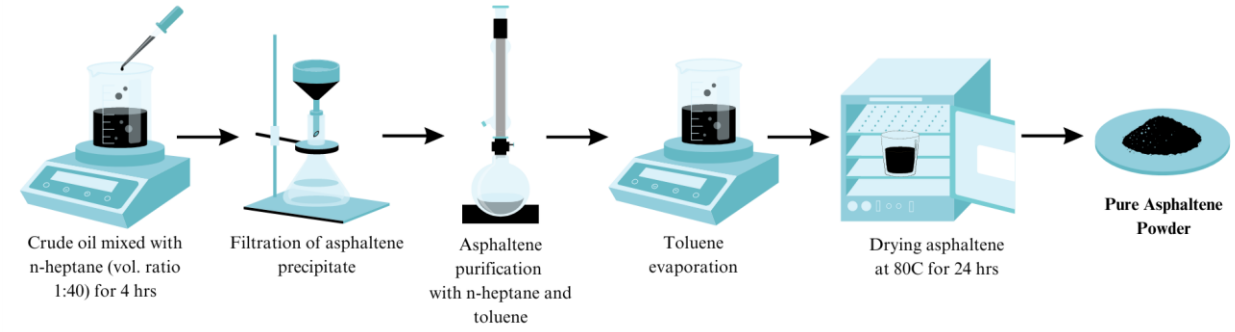

Figure 3-3. Illustration of asphaltene extraction procedure

The filter paper with precipitate on it is then placed in a Soxhlet apparatus and refluxed with hot *n*-heptane as shown in Figure 3-5. The reflux process continues until drops of *n*-heptane from the bottom of the extractor become pure. Afterward, the same procedure is repeated by replacing the *n*-heptane with toluene. As asphaltene is fully dissolved in toluene, the solution is put into the reflux container, which is placed in the oven for 24 hours at 80°C to evaporate the toluene and extract the pure asphaltene.

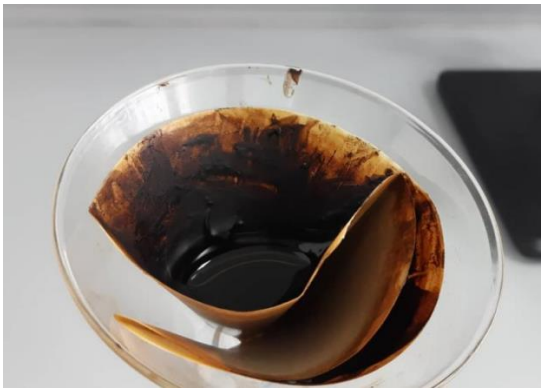

Figure 3-4. Filtration process of asphaltene precipitate.

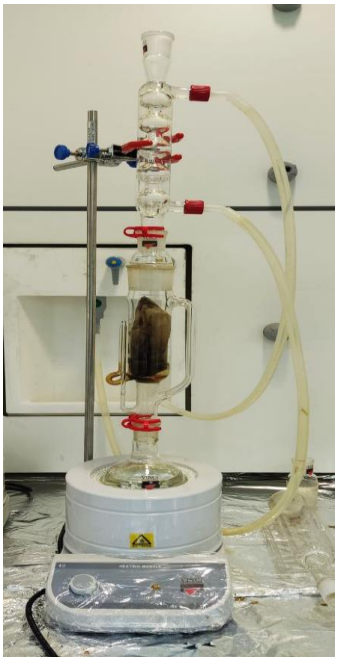

Figure 3-5. The Soxhlet apparatus used for asphaltene extraction.

3.4 Synthetic oil preparation

The following procedure is followed for preparation of synthetic oil which is used later for sample preparations. Asphaltene powder with 0.5 wt.% is added to a necessary amount of toluene. The mixture is stirred for at least 4 hours until the solid particles of the asphaltene completely dissolve in toluene. The obtained synthetic oil represents light oil due to low asphaltene content and consequently the density of the synthetic oil is assumed to be equal to toluene's density of 0.867 g/cc.

3.5 Asphaltene characterization

In this research work, there are two main techniques used to characterize the asphaltene extracted. The first technique is X-Ray Photoelectron Spectroscopy (XPS) and it was performed on the NEXSA apparatus by Thermo Scientific as shown in the Figure 3-6. The spectrometer's X-ray source type is Al kα ($hv = 1486.6\,eV$) and all obtained spectra were referenced to C-14 (h_v =284.8 eV). To obtain the asphaltene characteristics, the powder was spread with a thin layer on a double-sided tape which was pasted to the sample holder by the other side. The sample holder was then placed into the spectrometer and the results were received which required further interpretation. The analysis of the XPS results is presented in the Results and Discussion chapter.

Figure 3-6. XPS – NEXSA Spectrometer.

3.6 Characterization of the NPs/NC

There are multiple characterization techniques used to investigate NPs/NC properties on multiple levels. These techniques also include the application of XPS described in the asphaltene characterization and since NPs/NC have a powder form as asphaltene, the methodologies of sample preparation are identical.

The second technique is Fourier-Transform Infrared Spectroscopy (FTIR) and it was performed on Nicolet iS10 FT-IR Spectrometer by Thermo Scientific as shown in the Figure 3-7. The spectrometer operates in a spectral range of 7800 to 350 cm^{-1} with a resolution of 0.4 cm^{-1}. The characteristics are extracted by placing a little amount of asphaltene powder in the center of the diamond crystal of the ATR plate. The obtained results are discussed in the next chapter.

Figure 3-7. Nicolet iS10 FT-IR Spectrometer.

The other technique used is X-Ray Diffraction (XRD) and it is performed on Smart Lab (Rigaku) apparatus as shown in the Figure 3-8. To examine the crystal structure of a material, a small amount of powdered sample (about 5 mg) is put in a zero background sample holder with size of a 5 mm x 0.2 mm and fixed by a glass slide. The obtained spectrum of the diffraction intensity against diffraction angle is further analyzed based on peak types.

Figure 3-8. The XRD System - Smart Lab (Rigaku).

The next technique used is Scanning Electron Microscopy (SEM) performed on ZEISS Crossbeam 540 as shown in the Figure 3-9. The microscope allows to measure grain sizes of the NPs and NC. Sample preparation for the microscope is quite similar to the XPS, where a powdered sample is spread on a metallic tape and the sample must be additionally sputter coated with gold to prevent sample charging. The results of the SEM are obtained as high-quality images with resolutions up to 100 nm. The microscope additionally allows to perform Energy Dispersive X-Ray Spectroscopy (EDX) analysis.

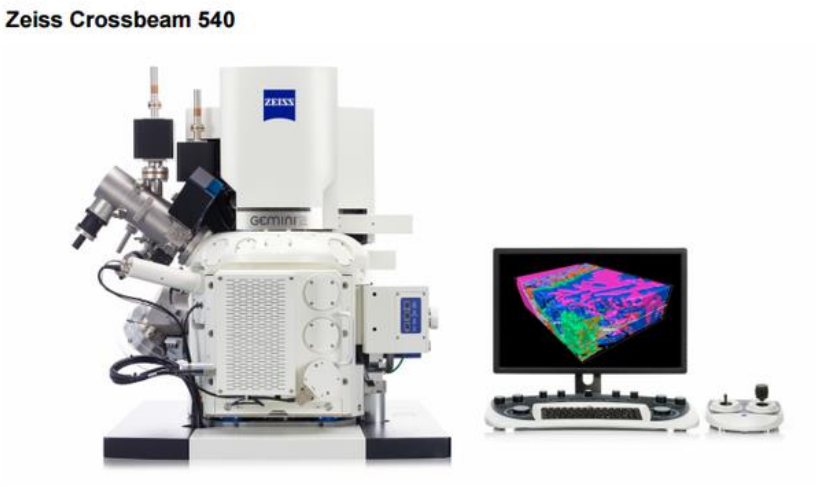

Figure 3-9. The SEM System – Zeiss Crossbeam 540.

Lastly, Transmission Electron Microscopy (TEM) performed on the JEOL JEM-1400 Plus apparatus (Figure 3-10) and used to determine the size and shape of the samples. Unlike other aforementioned techniques, the TEM is very sensitive to impurities in the samples and thus requires high attention during the sample preparation. A copper grid coated with amorphous carbon is used as the foundation for the sample. Each studied NP – SiO_2 and ZnO – was weighted to have a mass of 5 mg and was mixed with 10 ml of distilled water in presence of ultrasonic waves to achieve a homogeneous mixture. After this, one drop of the mixture was put on the grid and left for 24 hours to achieve complete adsorption. Afterward, the copper grids with fully adsorbed NPs/NC are put into the microscope and the obtained images are analyzed.

Figure 3-10. The TEM system – JEOL JEM - 1400 Plus.

3.7 Sample preparation method for asphaltene precipitation investigation

To evaluate precipitation of asphaltene in absence and presence of nanoparticles on the silica surface, two respective conditions are applied for preparations of the samples. Firstly, it is necessary to prepare synthetic oil according to the presented instructions. The next is developing two different conditions: one flask must contain only synthetic oil, whereas 0.1 wt. % of NP/NC is added to the second one in presence of ultrasonic waves. All of the following procedures are the same for both flasks. Afterward, to destabilize asphaltene in the oil and make it precipitate, co-solvent *n*-heptane is added in a volumetric ratio of 50:50 to the synthetic oil. Each prepared solution is then poured into a beaker each having a piece of the silica surface. Pieces of silica surface must be purified with acetone in presence of ultrasonic waves and then with distilled water in advance. Silica samples are left to age in the prepared solutions for 2 hours allowing unstable asphaltene to precipitate on the silica surface. After 2 hours, solutions must be drained from the beakers to leave the silica surfaces to dry in ambient conditions. Eventually, there should be four surfaces obtained for further analysis:

1. Silica surface after asphaltene precipitation in absence of NC/NP;
2. Silica surface after asphaltene precipitation in presence of SiO_2;
3. Silica surface after asphaltene precipitation in presence of ZnO;
4. Silica surface after asphaltene precipitation in presence of NC.

These surfaces are then examined by two different surface topography methods – Atomic Force Microscopy (AFM) and Contact Angle (CA) measurement technique. The sample preparation schematics is shown in Figure 3-15.

3.7.1 Evaluation of asphaltene precipitation by AFM

Application of the AFM for investigation of the effect NPs/NC on asphaltene precipitation on silica surface is described in this section. The Atomic Force Microscopy (AFM) is a powerful and acknowledged technique used to investigate various surfaces, their morphology, irregularities, and interactions that occur on them at high resolutions in a quantitative way (Tazikeh, et al., 2020; Kumar, et al., 2004). The AFM method is widely used because it does not spoil samples and allows re-use of them in other experiments, as well (Wang, et al., 2013). Moreover, this instrument allows for studying surfaces both in two-, and three-dimensions (Wang, et al., 2013).

The AFM has been performed on SmartSPM 1000 apparatus shown in Figure 3-11. Firstly, the sample is placed on a sample holder. The next step is selecting and attaching the cantilever (tip

used in scanning the sample surface) to the microscope. The cantilever characteristics used for this study are shown in Figure 3-12. The results of the microscope scanning are presented in 2- and 3-dimensional images with a surface area of 10µm x 10µm. The AFM images are obtained for pure silica surface and earlier prepared four surfaces (with and without NP/NC). By changing the position of the cantilever's tip, several AFM images for each surface sample can be obtained.

Figure 3-11. The AFM System – SmartSPM 1000.

Figure 3-12. Cantilever characteristics used for AFM.

3.7.2 Contact Angle Measurement

The contact angle measurement allows to observe the change of surface wettability due to asphaltene precipitation in presence/absence of NP/NC. As the contact angle decreases, the tendency for the aqueous phase to wet the surface increases. The contact angle is measured by the apparatus shown in Figure 3-13. The contact angle was determined using the sessile-drop technique. Substrate type is silica. The contact angle measurements depend on both pressure and temperature. Hence, it is necessary to specify the thermodynamic conditions (Seyyedi, et al., 2015). The software operated with the following conditions: ambient phase – air, drop phase – water, drop model – sessile-drop. One drop of distilled water is added to generate a two-phase fluid mixture. After that, a digital camera (USB digital microscope 1000X) is used to take a photo of the contact and image analyzing software calculates the contact angle (Tazikeh, et al., 2022). The software calculates the contact angle based on different fitting techniques – Circle, Ellipse, and Young-Laplace. The results of these fitting techniques are compared with each other and the most accurate is chosen.

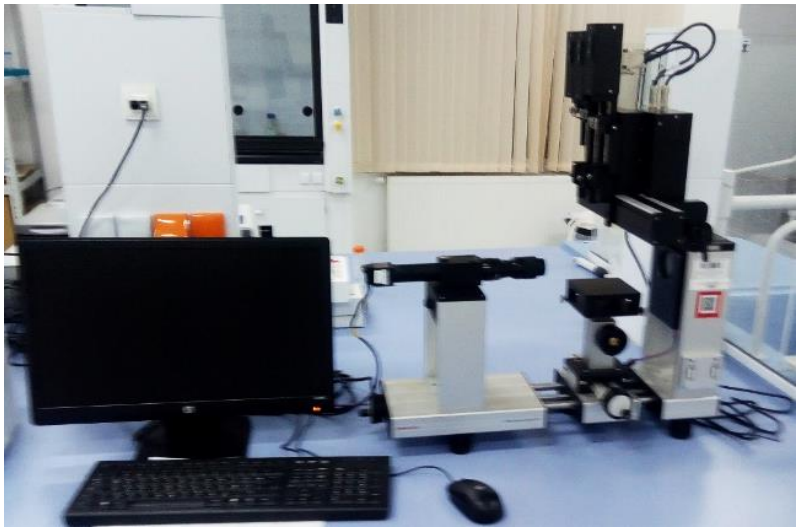

Figure 3-13. The contact angle goniometer.

3.8 Sample preparation method for investigation of asphaltene adsorption

To evaluate asphaltene adsorption in absence and presence of nanoparticles on the silica surface, two types of solutions must be prepared for each of the following cases: 1- silica surface only, 2- silica surface with NC, 3- silica surface with SiO_2, 4- silica surface with ZnO). Before starting to prepare the samples, it is important to purify pieces of the silica surfaces with acetone in presence

of ultrasonic waves and clean out them with distilled water. The solution must contain synthetic oil with 0.5 wt.% asphaltene content and co-solvent *n*-heptane with a respective volumetric ratio of 70:30. For the first case (silica surface only), the silica surface is vertically immersed into two solution of synthetic oil with *n*-heptane. For the cases with NPs/NC, 0.1 wt.% of the NP/NC must be added to each solution in presence of ultrasonic waves. Each container must be sealed and left to age for 72 hours as shown in Figure 3-14. Afterward, the solutions are drained and the pieces of silica surfaces are placed into vacuum oven immediately for 24 hours at 50°C. After 24 hours, the surfaces are fully dried and can be further used for XPS analysis. The sample preparation schematics is shown in Figure 3-15. Overall, 4 surfaces must be prepared:

1. Silica surface with synthetic oil and *n*-heptane
2. Silica surface with synthetic oil, *n*-heptane, and NC
3. Silica surface with synthetic oil, *n*-heptane, and SiO_2
4. Silica surface with synthetic oil, *n*-heptane, and ZnO

Figure 3-14. The samples prepared for investigation of asphaltene adsorption.

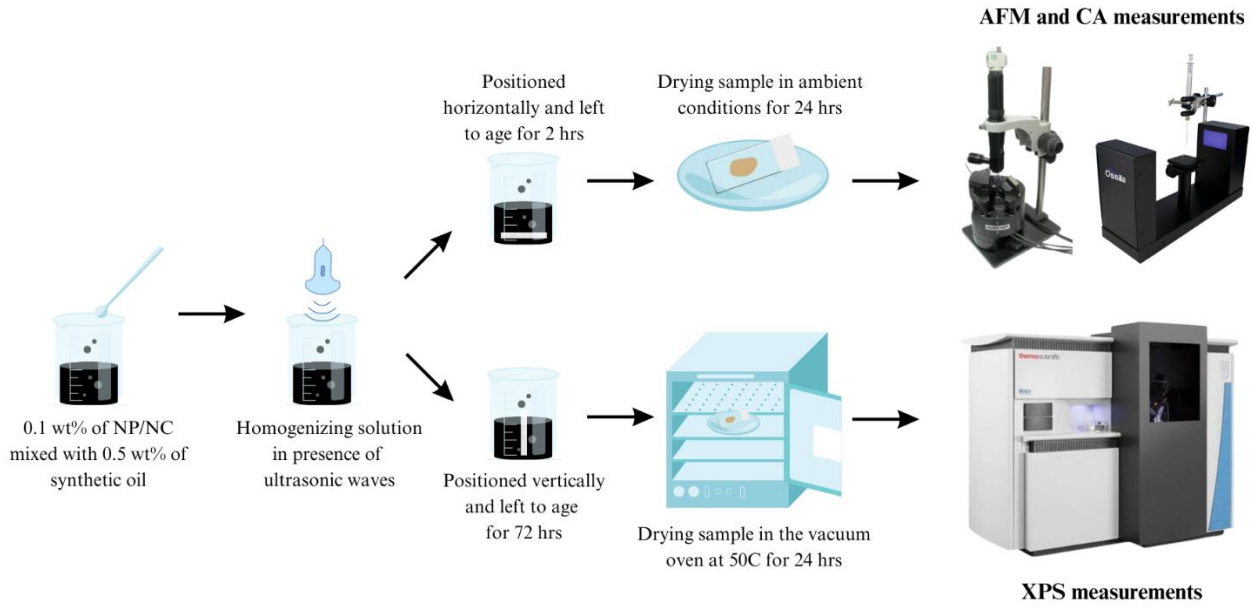

Figure 3-15. Illustration of sample preparation for AFM, CA, and XPS measurements

3.8.1 Evaluation of asphaltene adsorption by XPS

X-ray photoelectron spectroscopy (XPS) is highly accurate quantitative surface analysis technique used to identify chemical composition and state of a studied sample (Wang, et al., 2013). The accuracy of the XPS results is up to 10 nm in-depth. However, it tends to be limited up to 2-5 nm in depth (Wang, et al., 2013; 2016). The results of the XPS analysis are presented as a spectrum with peaks and corresponding chemical shifts (Abdallah & Taylor, 2008).

NEXSA Spectrometer used for asphaltene and NPs/NC characterization is also used for surface analysis of the silica samples. Eight prepared samples along with the pure silica surface are placed to a sample holder and fixed to it as shown in Figure 3-16. Additionally, it is important to reference chemical composition of each surface to Carbon-14 (hv=284.8 eV). The obtained chemical composition results are further examined using Thermo Avantage software which is specialized for interpretation of XPS spectrum. The results and their analysis are presented in Results and Discussion section.

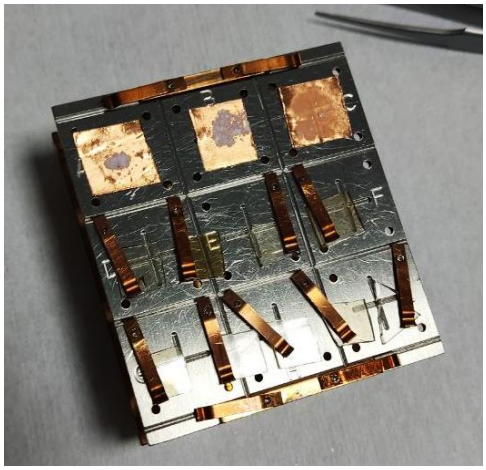

Figure 3-16. The samples prepared for XPS analysis.

4 Results and Discussion

The outcomes of each experimental part of this research are presented and discussed in this chapter. The findings of several modern analytical techniques used for NP/NC characterization including FTIR, TEM, XRD, SEM, and EDX are presented and discussed followed by interpretation and discussion of the AFM probes, CA measurements, and XPS surveys.

4.1 NP/NC characterization

4.1.1 FTIR Analysis

The FTIR spectrum for SiO_2 nanoparticle is presented in Figure 4-1. Spectrum contains small peak at 796 cm^{-1} and highly intensive peak at approximately 1080 cm^{-1}. The first one peak (about 796 cm^{-1}) identifies Si-O-Si symmetric stretching, while largest peak (about 1080 cm^{-1}) refers to Si-O-Si asymmetric stretching. The described stretching peaks show the presence of the Si-O functional group. The Si-O functional group is polar which is considered as an effective material for asphaltene adsorption.

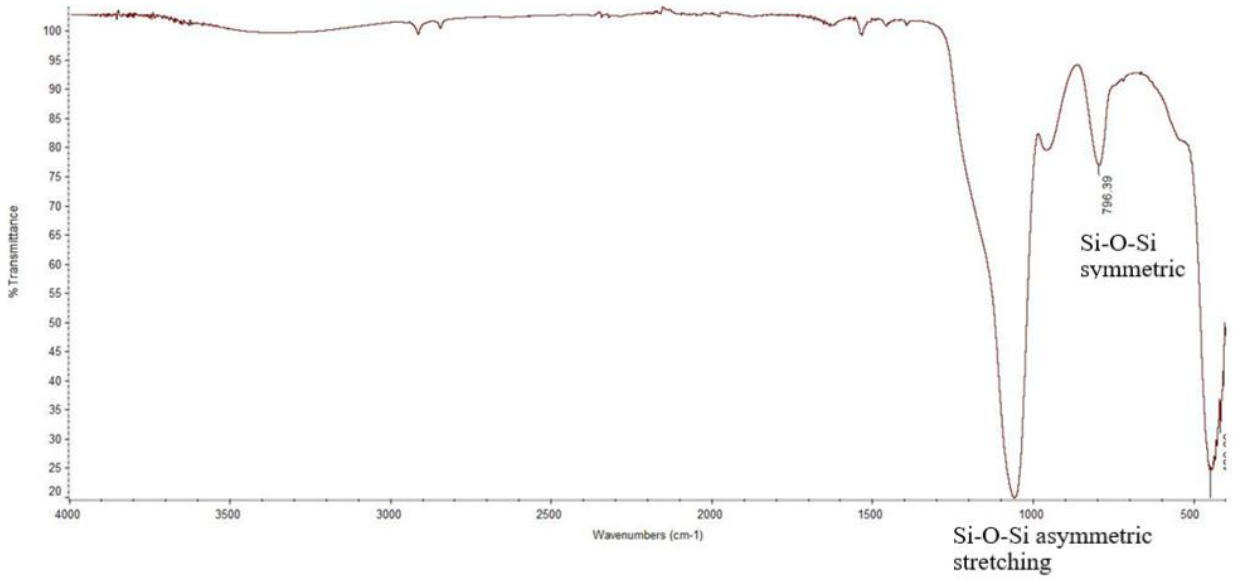

Figure 4-1. FTIR spectrum of SiO_2 NPs

The result of FTIR experiment with ZnO NP is presented in Figure 4-2. The spectrum contains highly intensive peak at wavenumber of about 450 cm^{-1} related to Zn-O bond.

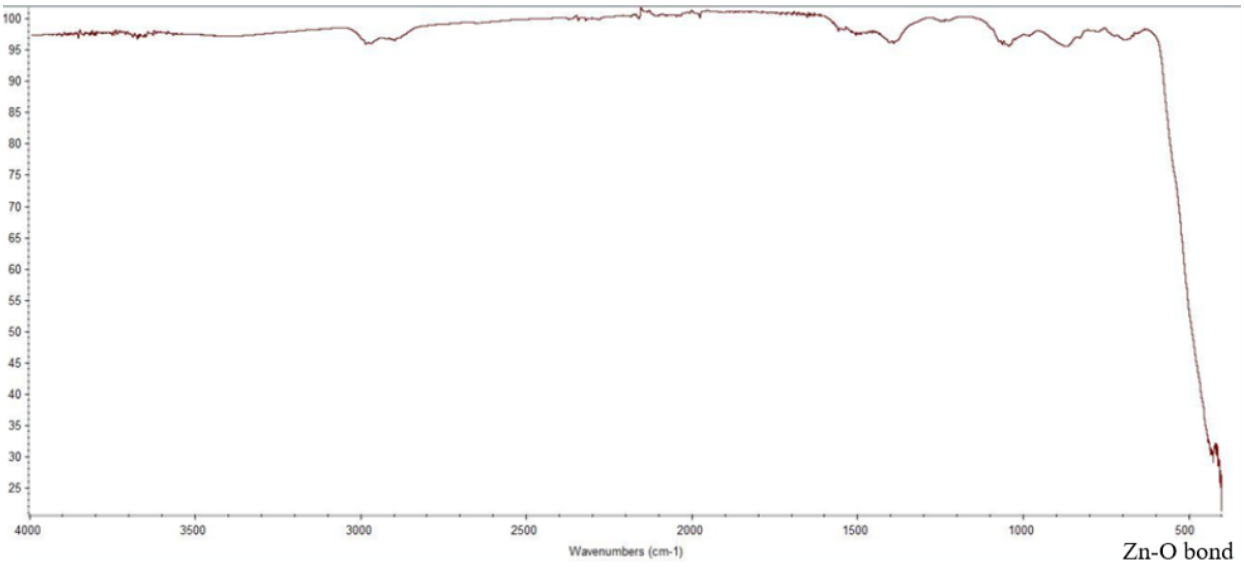

Figure 4-2. FTIR spectrum of ZnO NPs

The last FTIR spectrum presented in Figure 4-3 refers to ZnO-SiO_2-Thiazine nanocomposite. The spectrum contains both types of chemical bonds analyzed in the first two spectrums. From the given FTIR spectrum we can see the peaks about 406-440 cm^{-1} which refers to the Zn-O bond. The peak about 1069 cm^{-1} is related to Si-O-Si asymmetric stretching vibration in SiO_2 nanoparticle, and peak about 803 cm^{-1} is related to Si-O-Si symmetric stretching vibration. The vibrations of -CH_3, -C=C-H, =CH_2, -C-N, -C=C- functional groups are observed in the range of 1400-1700 cm^{-1} which is in the agreement with literature results (Si, et al., 2014).

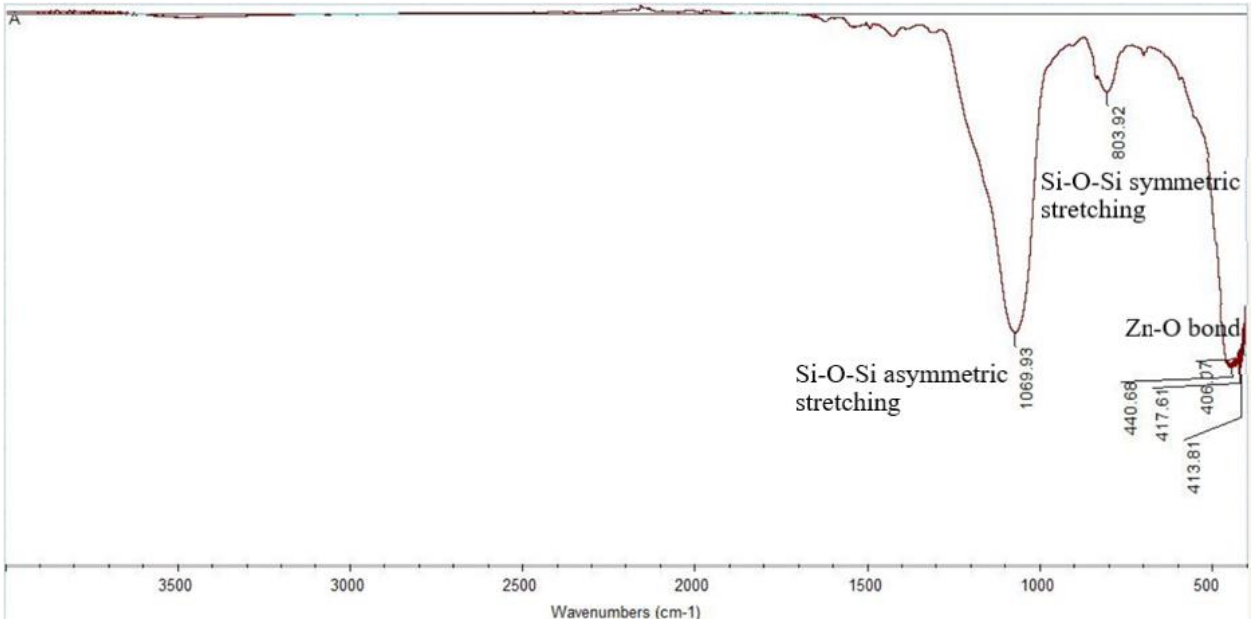

Figure 4-3. FTIR spectrum of ZnO-SiO_2-Thiazine NC

4.1.2 TEM Analysis

The following figures represent images obtained from TEM analysis. Figure 4-4a depicts TEM image of ZnO NPs from which interplanar spacing of about 25 nm and NP size of 20 nm can be observed. This observation is in agreement with SEM measurement results discussed further in this Chapter. TEM image of ZnO also reveals the spherical size of the NPs with diameter about 80 nm, forming large aggregates with size of 100-500 nm, which is also proved by SEM imaging.

From Figure 4-4b, it can be seen that SiO_2 NPs have much smaller molecules size compared to ZnO NPs. TEM image of ZnO-SiO_2-Thiazine NC in Figure 4-4c, reveals the average size of less than 50 nm. The structure of the particles is clearly seen in all of the samples' images. Small size of NPs/NC will assist asphaltene adsorption, since the smaller size allow the asphaltene molecules closer interact with the NPs/NC.

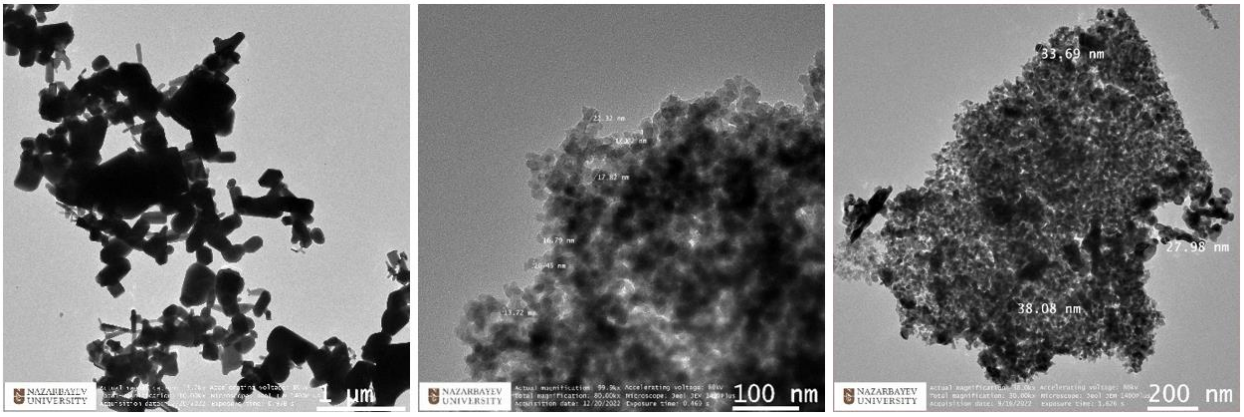

Figure 4-4. TEM images of a) ZnO NP, b) SiO_2 NP, and c) ZnO-SiO_2-Thiazine NC

4.1.3 XRD Analysis

X-ray diffraction experiment showed information about the chemical composition, crystallographic structure, and physical properties of a sample. In Figure 4-5, the result of the XRD measurement with SiO_2 NPs can be seen. The obtained spectrum shows low-intensive peaks with larger widths compared to ZnO NP. Low intensity tells about the small size of crystallites; while, ample width shows the large average crystalline size of SiO_2 NP.

The XRD spectrum of ZnO NP in Figure 4-6 showed distinctive multiple peaks at 30-40° which correspond to Zn-O bonds, and tell about zinc oxidewurtzite structure The intensity of the peaks is in the range of 50 000 – 24 000 cps, showing large size of ZnO crystallites, whereas small width presents small average size of ZnO crystalline. The XRD spectrum of ZnO-SiO_2-Thiazine NC in Figure 4-7 showed distinctive multiple peaks at 30-70° which show polycrystalline nature

of the NC. Also, low intensity of the peaks and low their small width correspond to small size of crystallites and crystalline respectively.

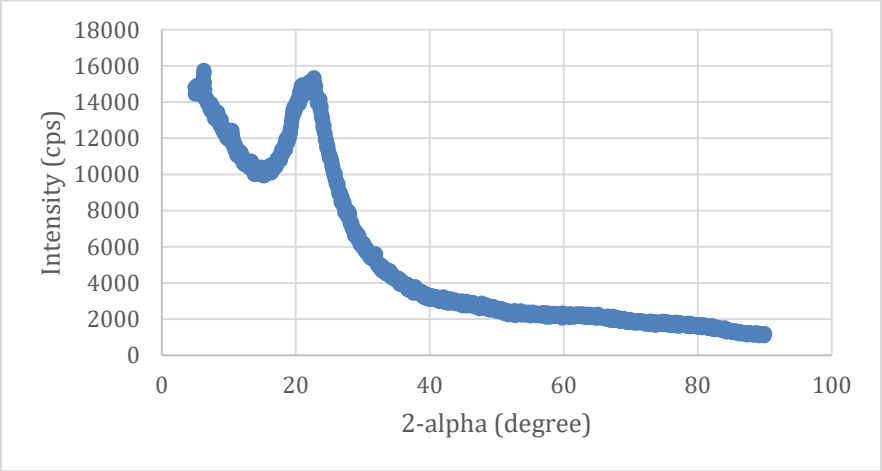

Figure 4-5. XRD Spectrum of SiO_2 NPs

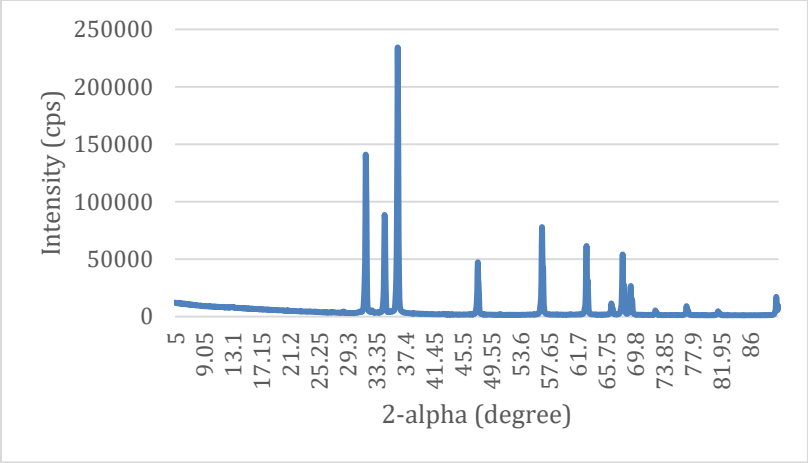

Figure 4-6. XRD Spectrum of ZnO NPs

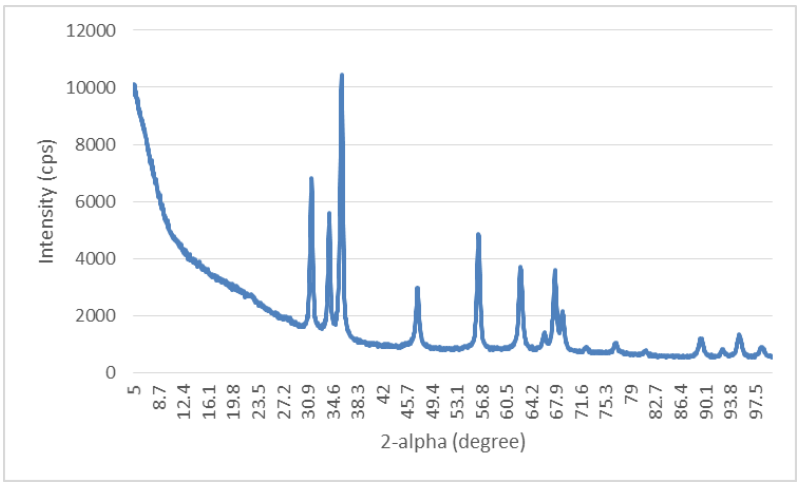

Figure 4-7. XRD Spectrum of ZnO-SiO_2-Thiazine NC

4.1.4 SEM Analysis

SEM image of ZnO NP is shown in Figure 4-8a. The shape of NPs is irregular and spherical, polycrystalline and long in one dimension (acicular). SEM image of SiO_2 NP (Figure 4-8b shows) demonstrates the irregular rod-shaped morphology and micro-flakes of NP. Figure 4-9 illustrates the SEM image of ZnO-SiO_2-Thiazine NC with average aggregate size 300-1000 nm. The aggregate size of nanocomposite is between sizes of ZnO and SiO_2 NPs.

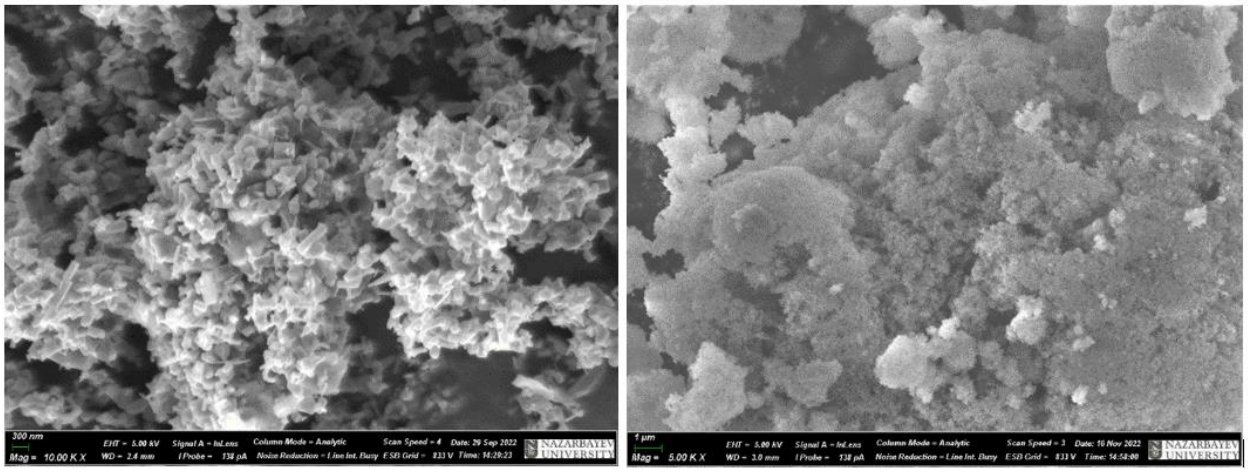

Figure 4-8. SEM image of a) ZnO and b) SiO_2 NPs

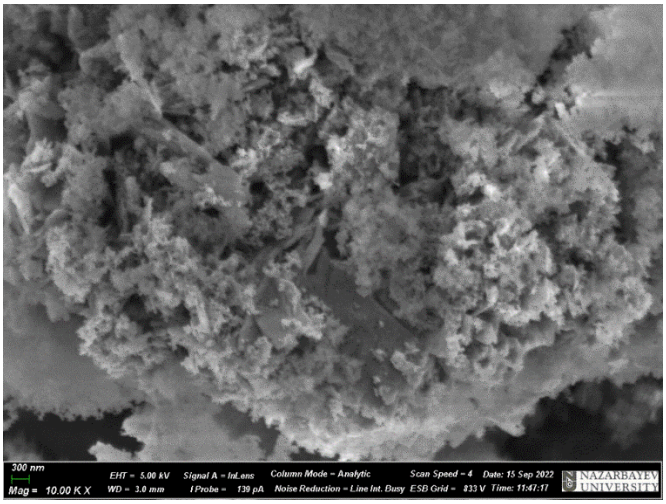

Figure 4-9. SEM image of ZnO-SiO_2-Thiazine NC

4.1.5 EDX Analysis

EDX spectrum of ZnO NP is presented in Figure 4-10. There are two major peaks in the spectrum – 55.1 wt% and 41.7 wt% corresponding to Zn and O atoms, respectively. The EDX spectrum of ZnO-SiO_2-Thiazine NC in Figure 4-11 illustrates multiple peaks of 42.7 wt%, 22.9 wt%, 17.0 wt%, 15.1 wt%, 1.9 wt%, and 0.3 wt%, corresponding to oxygen, silicon, zinc, carbon, sodium, and aluminum atoms respectively. The main three peaks such as oxygen, silicon, and zinc are in the agreement with the chemical formula of NC, the rest of the atoms are the impurities which may be resulted from the preparation stage.

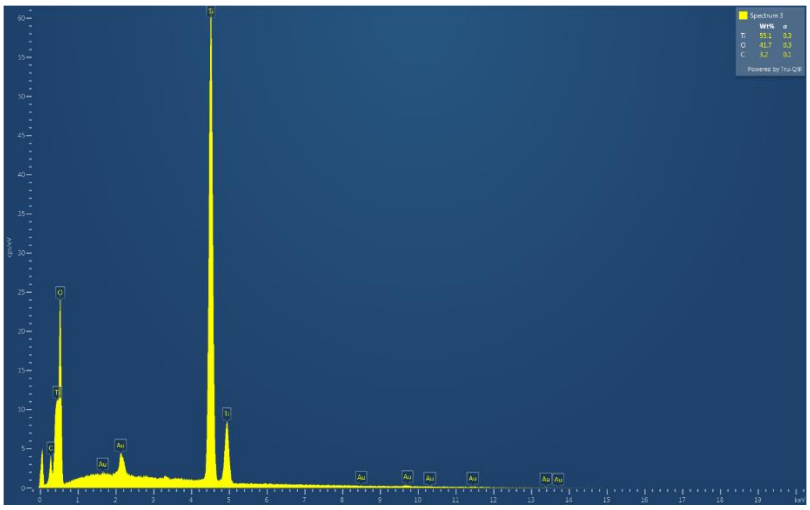

Figure 4-10. EDX Spectrum of ZnO NPs

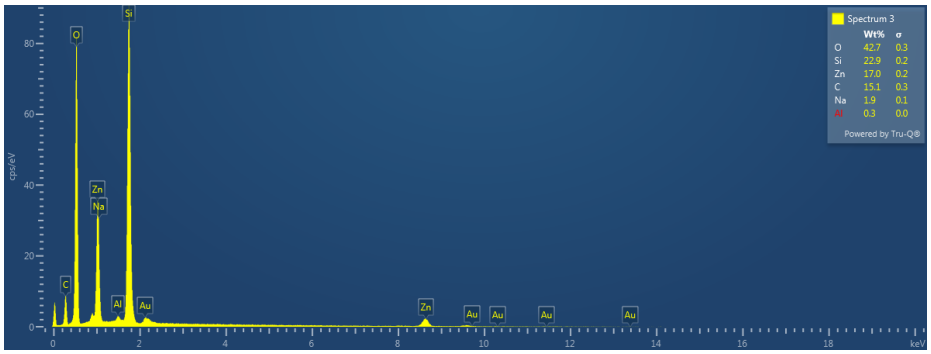

Figure 4-11. EDX Spectrum of ZnO-SiO_2-Thiazine NC

4.2 NP/NC effect on asphaltene precipitation

In order to analyze the amount of asphaltene precipitated onto silica surface, AFM images of sample surfaces with resolution of 10×10 µm are obtained. Figure 4-12 depicts AFM image of a pure silica surface. The surface is smooth with no precipitate or roughness.

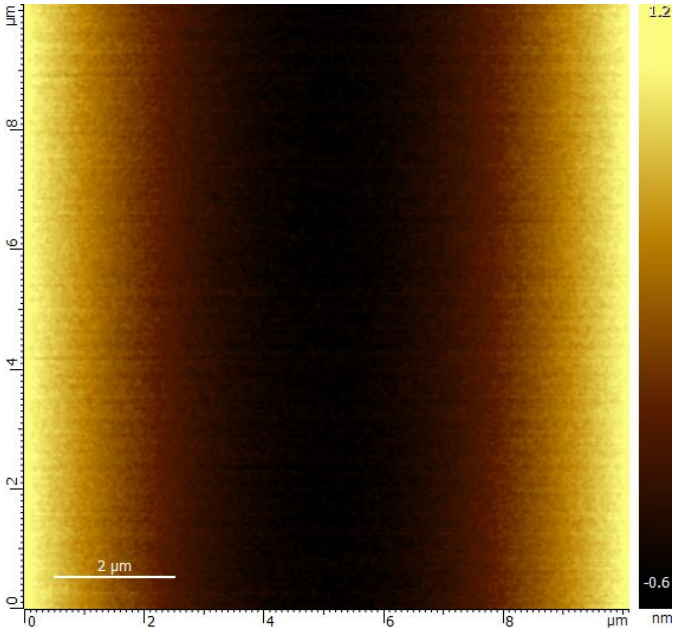

Figure 4-12. Pure Silica surface

Figures 4-13 (a-c) demonstrate silica surfaces with asphaltene precipitation on it. The height of asphaltene precipitate is approximately 100 nm. Additionally, based on the results it can be concluded that the type of precipitates are divided into 2 major types: big/tall precipitates and small/short precipitates.

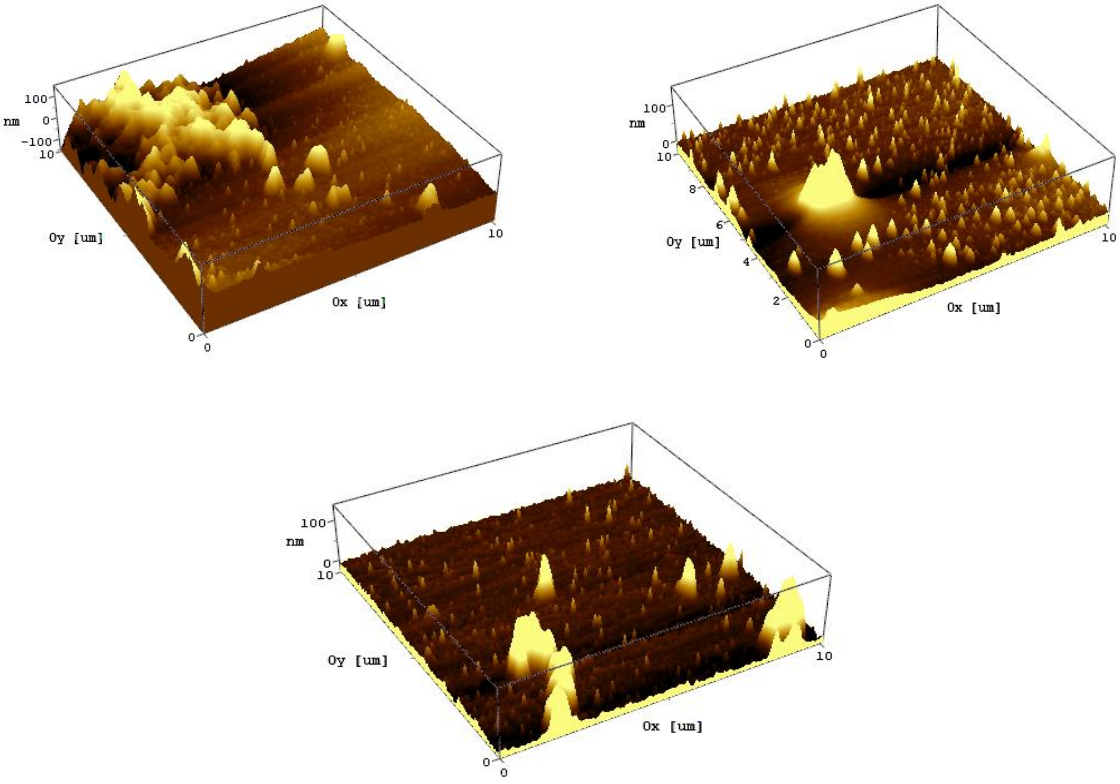

Figure 4-13. Silica surface after asphaltene precipitation in absence of NP/NC

Since the studied ZnO-SiO_2-Thiazine nanocomposite consists of 2 NPs - SiO_2 and ZnO - it is important to compare each of their effects on asphaltene adsorption separately. Figures 4-14 (a-b) demonstrate the silica surfaces after asphaltene precipitation in presence of SiO_2 nanoparticles. It can be seen that compared to Figures 4-13 (a-c), the number of asphaltene precipitates has been considerably reduced and peaks of asphaltene precipitation became thinner. Nevertheless, there are still short/small asphaltene precipitates present with a maximum height of less than 100 nm.

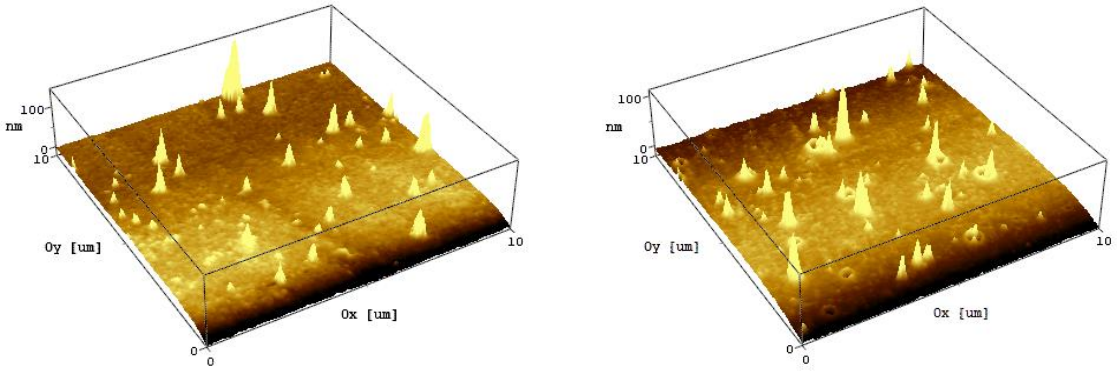

Figure 4-14. Silica surface after asphaltene precipitation in presence of SiO_2

Figures 4-15 (a-b) reveal the silica surface after asphaltene precipitation in presence of ZnO nanoparticles. Compared to SiO_2, it can be seen that ZnO tends to remove small/short precipitates rather than big ones. Therefore, in Figures 4-15 (a-b), a few big precipitates of a maximum height of 200 nm can be seen with no small/short precipitates.

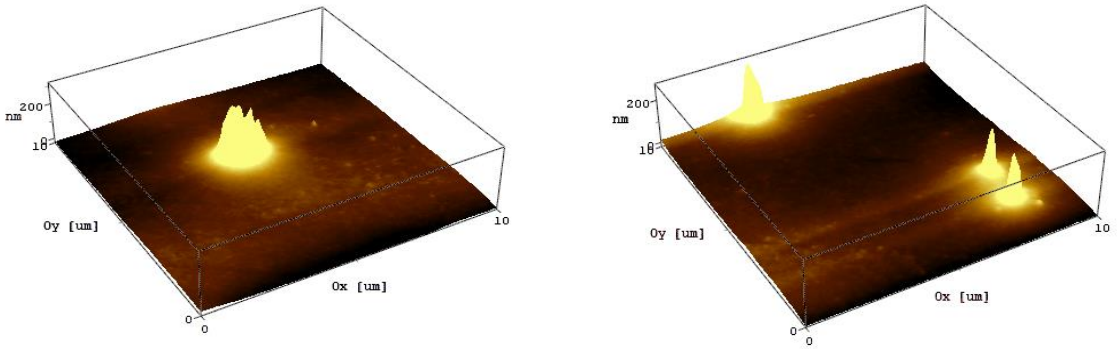

Figure 4-15. Silica surface after asphaltene precipitation in presence of ZnO

Therefore, to reach the combined effect of both nanoparticles, SiO_2-ZnO nanocomposite was prepared and its effect on asphaltene precipitation was studied. As it can be seen on Figure 4-16, the behavior of asphaltene precipitation in the presence of NC. It can be observed that there is no big precipitation as in Figures 4-13 (a-c), meaning that NC works. Moreover, the amount of numerous small/short precipitates also decreased in presence of NC and the height of peaks was also reduced to about 100 nm, demonstrating the synergetic effect of SiO_2 and ZnO.

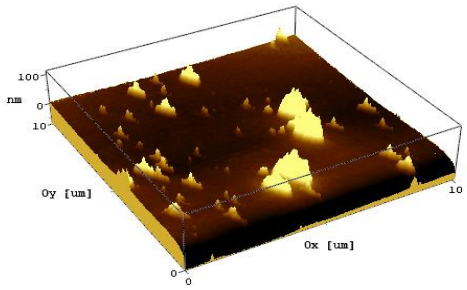

Figure 4-16. Silica surface after asphaltene precipitation in presence of NC

4.2.1 Surface topography: evaluation of roughness

The surface topography parameters obtained from AFM enable for a more precise evaluation of NP/NC performance by allowing for the quantitative definition and comparison of surface roughness. The results of calculations for all AFM surfaces presented in this chapter are included in Table 4-1 and the description of parameters is presented in *Section 2.8.1*.

From Table, it can be seen that the silica surface was pure enough, as its maximum and minimum height values are quite close and RMS is pretty low (0.0024 μm). The skewness, kurtosis and developed interfacial area ratio of the surface are nearly zero, meaning that the surface is smooth, nearly symmetrical with no peaks and valleys. It is evident that as asphaltene is precipitated on silica surface, the height extremely increases by almost 6 μm. This shift increases the difference between peaks and pits of the surface, making the surface rougher and the peaks sharper and asymmetric, which is also demonstrated by positive increase in S_{sk} and S_{ku}. The Developed Interfacial Area Ratio has increased by 2.6%, meaning that the surface more textured and rough. As SiO_2 is added to the surface, the height of the peaks decreases by about 0.8 μm. The decrease of S_a and S_q by 0.8 μm and 0.03 μm indicate the surface flatness in presence of NP. These decrease has also contributed to S_{dr} decrease up to 0.21%. Additionally, skewness and kurtosis become negative, thus exposing the stretched and slightly tilted nature of the asphaltene peaks. The addition of ZnO has not decreased the amount of asphaltene considerably, as S_a decreased only by 0.2 μm, whereas S_q increased up to 0.45 μm, meaning that the height of precipitates increased and became more disordered. Kurtosis, compared to SiO_2, became more negative indicating skewed surface with remote peaks. Eventually, S_{dr} in presence of ZnO reaches 1.4% due to high asphaltene peaks, though the spacing between them is wide enough.

Finally, the addition of NC has resulted in the most positive results. The height of peaks has decreased by almost 1.30 µm. Nevertheless, S_y and S_q has not decreased considerably, comparing to NPs, meaning that NC has less effect on the height distribution. However, the decrease of S_{dr} up to 0.67% is an indication of decreased texture effect with wider spaced peaks. Kurtosis and skewness are negative revealing the stretched and somewhat slanted form of the asphaltene peaks.

Table 4-1. Surface topography parameters in absence and presence of NP/NC

	Pure Silica	Si+Asph	Si+Asph+SiO_2	Si+Asph+ZnO	Si+Asph+NC
Maximum Peak Height (S_p), µm	-3.23143	2.52292	1.53242	2.8285	1.24747
Minimum Pit Height (S_v), µm	-3.24353	2.08438	1.30756	1.17917	0.944002
Arithmetical Mean Height (S_a), µm	-3.24001	2.23437	1.41639	2.0263	1.0734
Z Value Range (S_y), µm	0.0121	0.43854	0.22486	1.64933	0.303468
Root Mean Square Height (S_q), µm	0.0024394	0.0739816	0.0449242	0.453498	0.0612669
Skewness (S_{sk})	0.714632	1.29911	-0.0520762	-0.0610487	-0.0146857
Kurtosis (S_{ku})	-0.161063	1.07496	-0.672187	-1.18031	-1.11777
Developed Interfacial Area Ratio (S_{dr})	3.93538E-5	0.0261113	0.00208661	0.013919645	0.006778694

4.3 NP/NC effect on wettability alteration

Since, the main indicator of surface wettability is contact angle, the following obtained results summarized in Figure 4-17, 18 are used to analyze the wettability alteration of a silica surface due to asphaltene precipitation and NP/NC presence. Figure 4-17 shows silica surface before and after asphaltene precipitation and in presence and absence of NP/NC. Firstly, Figure 4-17a illustrates a pure silica surface with a droplet of water on it with CA of 19.7° which is much smaller 75°, thus representing absolutely water-wet surface. Figure 4-17b depicts a water droplet on a silica surface with asphaltene precipitates on it. It can be seen that the wetting behavior of a surface has drastically changed from water-wet to oil-wet with CA of 154.8°. This wettability alteration

confirms the undesirable effect of asphaltene precipitation of a rock surface making it oil-wet, thus hindering the oil production.

The next step is the addition of SiO_2 and ZnO nanoparticles separately, in order to evaluate their effect on the wettability of the silica surface after asphaltene precipitation. Figures 4-17 (c-d) reveal the surface response to the presence of SiO_2 and ZnO nanoparticles after asphaltene precipitation, respectively. Compared to Figure 4-17b, the surface has become more favorable to wetting by changing its property from oil-wet to intermediate-wet due to reduced value of CA of 100.8° for ZnO, SiO_2 remained to be oil-wet due to CA of 115.3°. Based on the CA results, it is evident that ZnO is more powerful in recovering the surface wettability than SiO_2 which can be explained by their working mechanisms at nanoscale. In Figures 4-14, 15 and Table 4-1, AFM results proved that though SiO_2 removes the big/tall precipitates, there are still numerous small/short precipitates all over the surface which conjunctionally may generate more oil-wet surface compared to ZnO. This can be explained by the fact that ZnO removes small precipitates, leaving high ones only, thus decreasing the peak spacing, which is eventually positively affecting wettability of the surface. However, the appliance of nanoparticles separately is still insufficient to refine the surface completely back to initial condition.

Finally, Figure 4-17e depicts the effect of NC on the silica surface after asphaltene precipitation. It is readily apparent that the surface has become much more favorable to wetting compared to results obtained from NPs – CA has reduced to 59.0°. Though the surface has not returned to its initial state in presence of NC from a surface roughness perspective, which is evident from Figure 4-16 and Table 4-1, it has successfully recovered in terms of surface wettability by becoming water-wet again as shown in Figure 4-17e. Thus, these obtained results have demonstrated the efficiency of the studied NC as a successful asphaltene inhibitor.

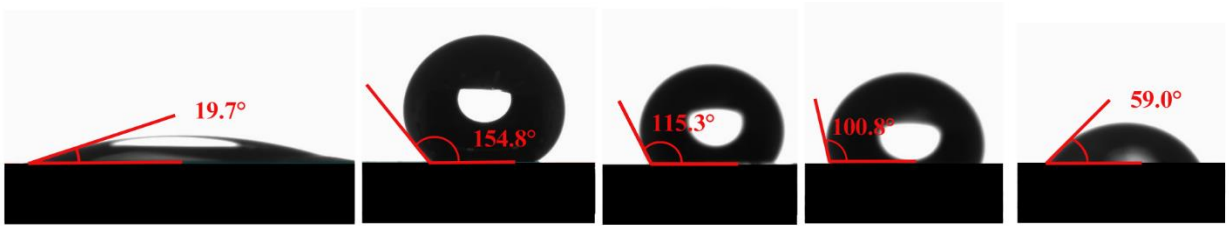

Figure 4-17. Wettability of Silica surfaces in presence/absence of NP/NC

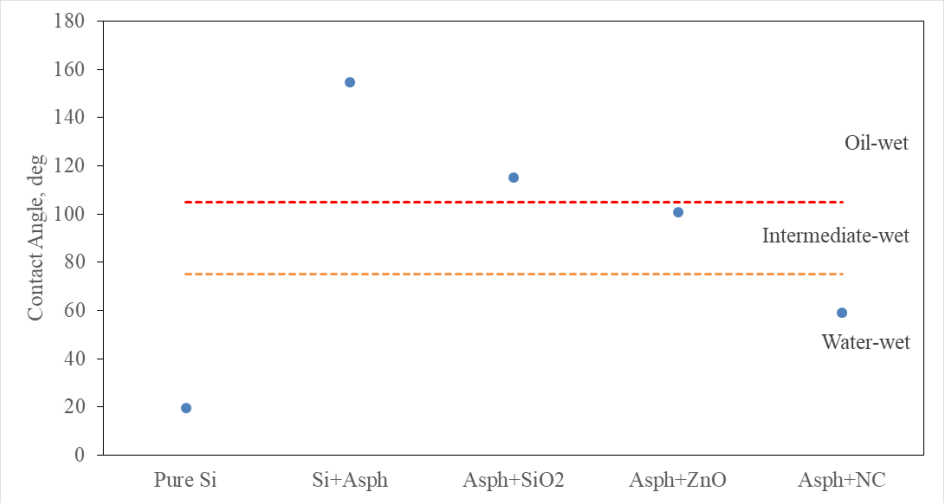

Figure 4-18. Contact angles of Silica surface in absence/presence of NP/NC

4.4 NP/NC effect on Asphaltene Adsorption

In order to analyze the extent of asphaltene adsorption onto silica surfaces in the absence/presence of NC/NP, the XPS analysis has been performed. Additionally, an XPS survey has been conducted on the pure silica surface itself along with the separately pure asphaltene, NPs, and NC each in powder form. Firstly, before analyzing silica surface samples for asphaltene adsorption, it is important define atomic compositions of a pure silica surface, ZnO and SiO_2 NPs, NC, and asphaltene powder.

4.4.1 XPS analysis of Silica surface

The overall XPS Survey analysis of a Pure Silica surface is presented in Figure 4-19. Since the chemical formula of silica is SiO_2, theoretically, the predominant element present in Silica must be O1s, with atomic ratio of twice bigger than Si2p. The theoretical hypothesis corresponds to the obtained results as shown in Figure 4-19 and the detailed elemental analysis is presented in Table 4-2. It should be noted that the presence of C1s is a common practice used as a charge reference for XPS surveys.

Table 4-2. XPS analysis of Pure Silica surface

Element	Binding energy (eV)	Atomic ratio (%)
O1s	532.32	49.63
Si2p	105.27	24.02
C1s	286.33	26.35

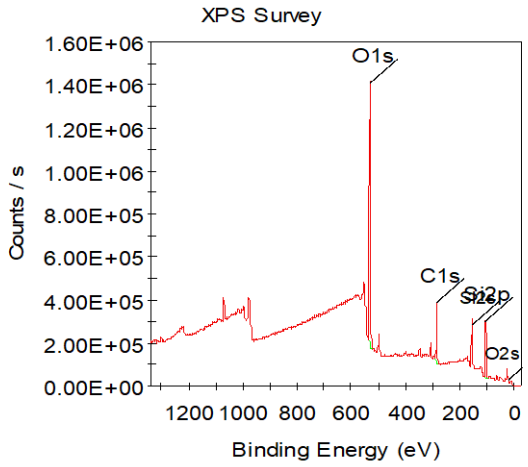

Figure 4-19. XPS Survey of Pure Silica surface

4.4.2 XPS analysis of NPs and NC

ZnO and SiO_2 NPs along with the ZnO-SiO_2-Thiazine NC has been analyzed by XPS and the survey results are presented in Figures 4-20 (a-c), whereas their elemental analysis is summarized in Table 4-3. The obtained XPS results for NPs prove the presence of all necessary bondings such as Zn-O metal bonding and O-Si-O bonding, thus their purity by the peaks at the corresponding binding energies and atomic ratios. As far as NC is concerned, since it has complex chemical composition, it is essential to examine its XPS result in details. Elemental analysis should be performed to identify chemical states of atoms present in NC, thus discovering its chemical structure. The results of elemental analysis are summarized in Table 4-4. From Table 4-3, it is evident that NC mostly constitutes of O 1s which exists in metal oxides (SiO_2, ZnO), hydroxides (-OH) and carboxylic/carbonyl groups. The next most abundant element is Si2p (more than quarter of NC composition) which exists in extracted SiO_2, whereas atomic ratio of Zn2p is about 5 times less than of Si2p composition. Additionally, there is about 13% C1s content present in NC. The chemical states of C1s are only sp2-, sp3-hybridized. Finally, about 1.5% of N1s is present in NC with various chemical states of pyridines (-C_5H_5N), pyrroles (-C_4H_4NH), and nitriles (-C≡N).

Table 4-3. XPS analysis of NPs and NC

	Binding energy (eV)			Atomic ratio (%)		
Element/ NPs and NC	ZnO	SiO_2	ZnO-SiO_2-Thiazine	ZnO	SiO_2	ZnO-SiO_2-Thiazine
C1s	285.11	286.23	286.31	31.36	6.13	12.89
O1s	530.42	533.92	533.19	41.87	61.65	55.46
Zn2p	1021.17	0.00	1021.99	26.77	0.00	3.37
Si2p	0.00	105.38	104.78	0.00	32.22	26.74
N1s	0.00	0.00	402.08	0.00	0.00	1.54

Table 4-4. XPS analysis of ZnO-SiO_2-Thiazine NC

Element	Chemical state	Binding energy (eV)	Atomic ratio (%)
Si2p	Partially oxidized, Si-O-Si	102.14	28.89
	Fully oxidized, SiO_2	103.53	71.11
C1s	C-C, C-H	284.84	70.4
	C=C, C=N	285.28	29.6
N1s	Pyridine,-C5H5N	398.36	3.13
	Pyrrole,-C4H4NH	398.66	85.95
	Nitrile, -C≡N	399.42	10.92
O1s	Metal oxides	530.2	30.53
	Hydroxides, -OH	531.22	36.13
	COO-	532.25	33.34
Zn2p	Zn metal	1020.44	49.4
	ZnO	1043.49	50.6

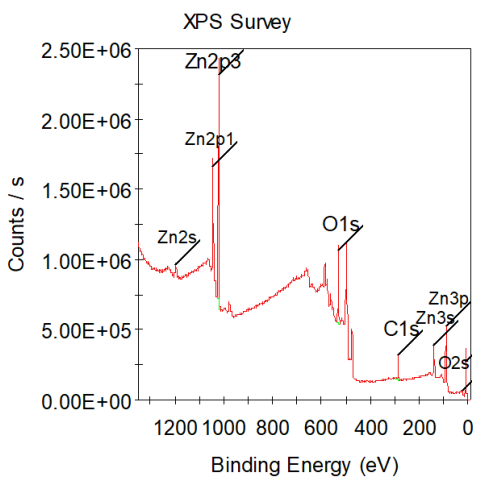

(a) XPS Survey of ZnO NPs

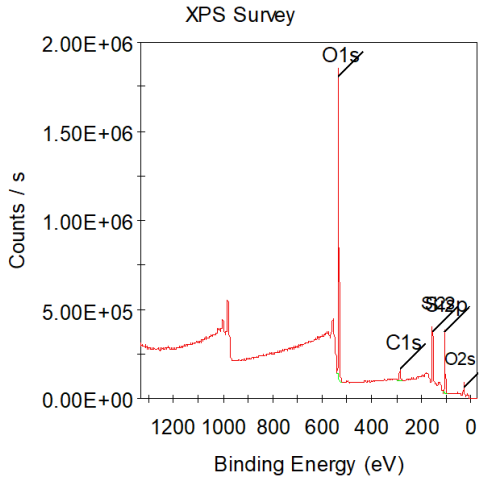

(b) XPS Survey of SiO2 NPs

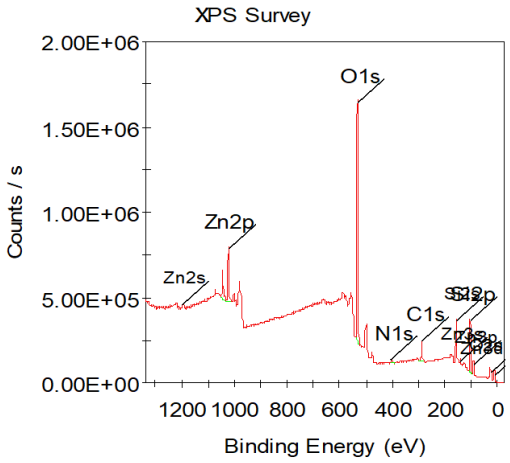

(c) XPS Survey of ZnO@SiO2@Thiazine NC

Figure 4-20. XPS Survey of NPs and NC

4.4.3 XPS analysis of Asphaltene

The overall XPS Survey of Asphaltene is shown in Figure 4-21 and its elemental analysis is summarized in Table 4-5. It can be seen that the XPS analysis has indicated the presence of C1s, O1s, N1s, and S2p elements in asphaltene powder. According to the survey conducted, about 85% of asphaltene constitutes of carbon atoms sp3 (C-C, C-H) and sp2 (C=C, C=N, C=O) hybridized chemical states. The presence of these bonds is verified by chemical states of oxygen atoms which make up about 12% of total asphaltene content. Oxygen atom is present in chemical states such as

C-O, C=O, carbonyl (C-O-C) and carboxyl (COO-) group. Additionally, extracted asphaltene powder also contains highly oxidized state of oxygen – peroxides (-O-O-).

Furthermore, asphaltene is also known as a crude oil fraction containing heteroatoms which are found to be sulfur and nitrogen in this case. Each of these heteroatoms compose less than 2% of total asphaltene content. According to the XPS spectrum, sulfur exists in asphaltene in numerous chemical states such as thiols (-SH), sulfides (-S-), sulfoxides (=S=O), sulfones ($-SO_3-$), sulfates ($-OSO_2-$), and sulfonates ($-SO_3-$). The similar variety of chemical states can be observed for nitrogen which are amines ($-NH_2$), amides (-NH-), pyridines ($-C_5H_5N$), pyrroles ($-C_4H_4NH$), imines (=NH), nitriles (-C≡N), and nitro groups ($-NO_2$).

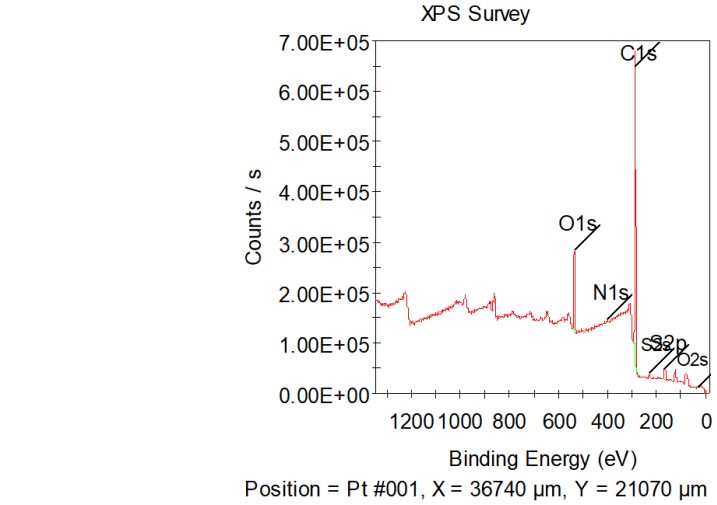

(a) Overall XPS Survey of Asphaltene

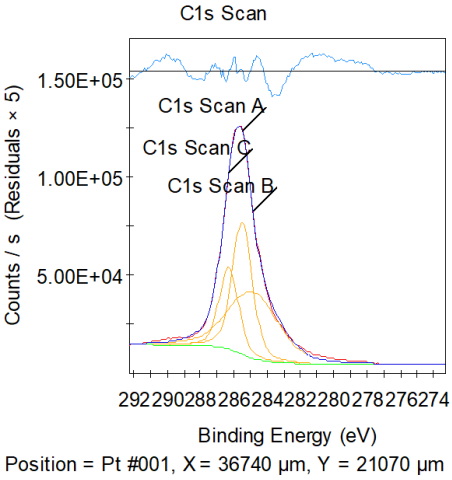

(b) XPS Survey of C1s

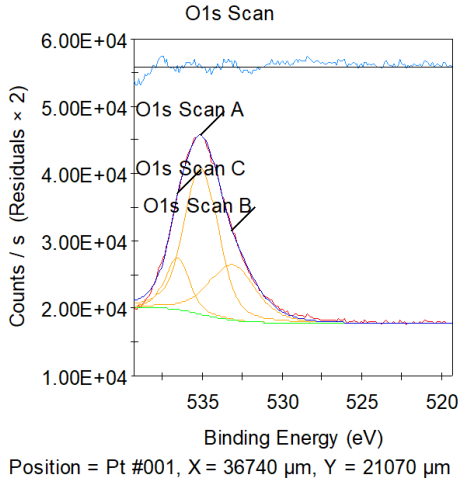

(c) XPS Survey of O1s

Figure 4-21. XPS Survey of Asphaltene

Table 4-5. XPS analysis of Asphaltene powder

Element	Chemical state	Binding energy (eV)	Atomic ratio (%)	Overall Binding energy (eV)	Overall Atomic ratio (%)
C1s	C-C, C-H	284.84	43.56	286.04	84.55
	C=C, C=N	285.49	35.48		
	C=O	286.3	20.96		
O1s	C=O, C-O, C-O-C	533.12	29.31	535.19	12.41
	Carboxyl group, COO-	535.08	56.68		
	Peroxide, -O-O-	536.57	14.02		
S2p	Thiol group, -SH	163.89	17.42	165.82	1.71
	Sulfide, -S-	164.51	22.14		
	Sulfoxide, =S=O	165.46	35.45		
	Sulfonate group, $-SO_3-$	166.49	25		
N1s	Pyridine, $-C_5H_5N$	396.68	17.62	400.74	1.33
	Pyrrole, $-C_4H_4NH$	399.67	42.2		
	Quaternary-N	401.31	38.57		
	Nitro group, $-NO_2$	403.75	1.61		

4.4.4 XPS analysis of Asphaltene adsorption in absence/presence of NP/NC

First of all, XPS Survey is conducted on a silica surface with asphaltene adsorption in the absence of NP/NC. The results of asphaltene adsorption, in form of synthetic oil, are summarized in Table 4-6 in the column designated “Asph”. From the Table, it can be seen that compared to the asphaltene in powder form, the overall atomic ratio of carbon atoms has increased up to 94%, whereas the amount of oxygen atoms has reduced by less than 3%. These changes can be explained by the fact that polar and aromatic molecules were adsorbed onto the silica surface, thus slightly changing the chemical states of C1s and O1s elements. On the contrary, the amount of sulfur and nitrogen has not experienced considerable changes. There is also 0.25% of silicon content present in the results which correspond to the silica surface itself. From now on, the XPS survey of

synthetic oil adsorbed onto silica surface is considered as an initial state and the following results are compared to the column “Asph”.

The next step is the addition of SiO_2 and ZnO NPs and ZnO-SiO_2-Thiazine NC to the silica surfaces and the evaluation of the intensity of asphaltene adsorption. The XPS survey results of these samples are depicted in Figure 4-22 (a-d) and summarized in Table 4-6 and presented in respective columns “Asph+SiO_2”, “Asph+ZnO”, and “Asph+NC”.

As NPs and NC were added, it can be seen that the overall atomic ratio of C1s is reduced, while O1s is increased. Though this trend can be observed for all cases, it can be noted that the application of NC results in greater changes than NPs application – C1s has decreased by 6.5% and O1s increased up to 3.1% for NC, whereas with NPs decreased C1s content by 0.3-2.0% and increased O1s content by 0.9%. Because carbon is the most abundant element in asphaltene, it is reasonable to conclude that the amount of asphaltene adsorption onto the surface reduced in the presence of NP/NC due to lesser carbon.

On the contrary, the decreasing tendency with the addition of NPs/NC can be noticed for S2p, where the most reduction is observed for NC – 0.5%, and less than 0.1% for NPs. This tendency can be explained by the reaction of asphaltene’s sulfur-containing functional groups and metals present in NPs/NC, which may result in the formation of metal-sulfur bonds. Additionally, it can be seen that N1s of NC by up to 1.5%, which can be explained by the chemical structure of Thiazine containing nitrogen atoms which were introduced to the surface. Overall, the addition of NPs/NC has caused changes in chemical composition of asphaltene/silica surface. The most drastic chemical modification is observed for NC, whereas ZnO, compared to SiO_2, is the least one to cause alterations.

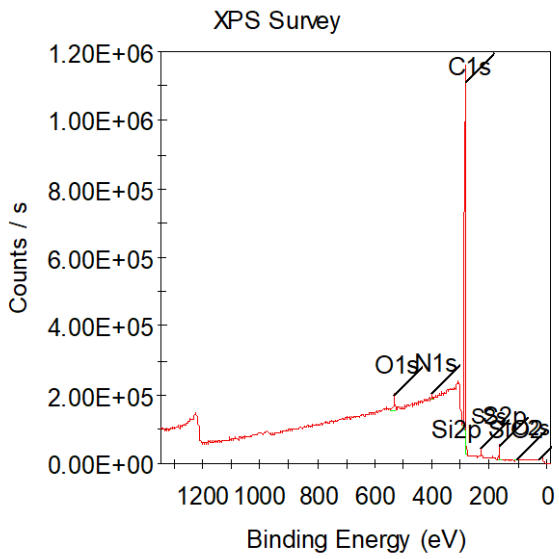

(a) XPS Survey of Asph

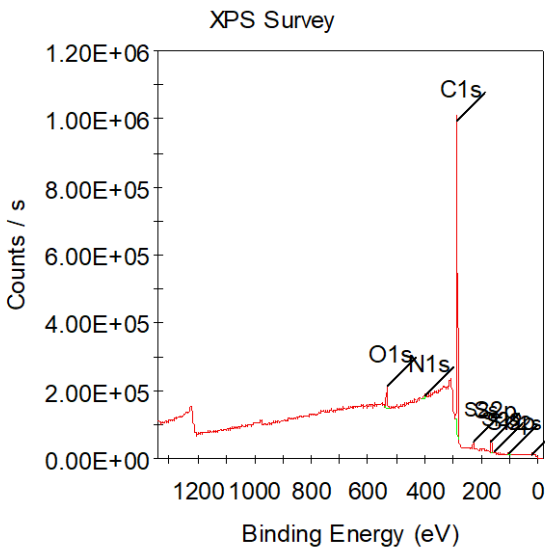

(b) XPS Survey of Asph+SiO_2

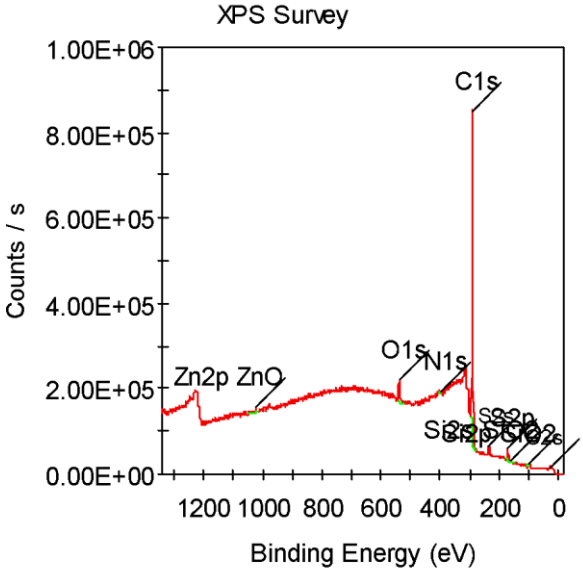

(c) XPS Survey of Asph+ZnO

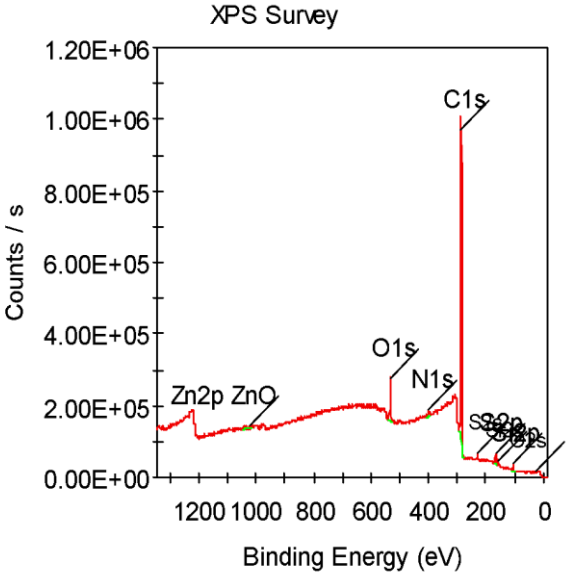

(d) XPS Survey of Asph+NC

Figure 4-22. XPS Survey of asphaltene adsorbed silica surface in absence/presence of NP/NC

Table 4-6. XPS survey of the silica surfaces after asphaltene adsorption in absence and presence of NPs and NC

Element	Chemical state	Binding energy (eV)				Atomic ratio (%)			
		Asph	Asph +SiO_2	Asph + ZnO	Asph + NC	Asph	Asph +SiO_2	Asph +ZnO	Asph + NC
C1s	C-C, C-H	284.28	284.78	284.84	284.83	27.45	37.84	23.71	23.04
	C-O, C-N	284.81	285.08	285.99	285.50	28.72	26.90	51.37	70.24
	C=O	285.39	285.70	286.77	286.02	43.82	35.26	24.92	6.72
	Overall C1s	**284.84**	**284.27**	**290.15**	**285.81**	**93.71**	**91.78**	**93.40**	**87.27**
O1s	Carbonyl, C=O	530.87	531.28	531.38	532.29	2.68	12.79	17.34	30.81
	C-OH, C-O, C-O-C	531.99	533.08	533.15	533.37	28.68	77.31	70.95	39.39
	COO-	532.77	534.48	534.68	534.43	68.64	9.90	11.70	29.79
	Overall O1s	**532.22**	**532.16**	**536.48**	**533.77**	**2.76**	**3.68**	**3.67**	**5.85**
S2p	Thiol group, -SH	163.71	163.32	157.06	156.46	12.13	27.59	16.11	11.08
	Sulfide, -S-	164.15	163.41	164.26	164.55	35.53	19.78	10.26	32.84
	Sulfoxide, =S=O	164.38	164.15	166.68	164.94	18.1	50.30	62.49	41.37
	Sulfonate, -SO_3-	165.20	165.29	167.66	166.20	34.24	25.58	11.14	14.71
	Overall S2p	**164.27**	**163.97**	**170.38**	**165.27**	**2.05**	**1.96**	**2.05**	**1.59**
N1s	Pyridine,-C_5H_5N	397.43	396.09	397.55	397.58	13.14	7.46	14.55	12.22
	Pyrrole,-C_4H_4NH	398.68	398.89	399.68	399.35	15.31	22.45	37.32	20.39
	Quaternary-N	400.23	400.52	401.08	400.82	58.28	55.42	45.18	57.44
	Nitro group, -NO_2	406.13	406.42	402.62	402.71	13.27	14.67	2.95	9.95
	Overall N1s	**399.57**	**399.03**	**399.20**	**401.02**	**1.23**	**1.55**	**0.22**	**2.63**
Si2p	Partially oxidized, Si-O-Si	102.58	102.52	93.65	104.07	73.43	73.53	53.11	46.93
	Fully oxidized, SiO_2	106.24	104.08	96.19	105.39	26.57	26.47	46.89	53.07
	Overall Si2p	**102.34**	**103.26**	**94.84**	**105.04**	**0.25**	**1.03**	**0.5**	**2.53**
Zn2p	Zn metal	0.00	0.00	1022	1023.04	0.00	0.00	73.27	58.83
	ZnO	0.00	0.00	1044.78	1045.80	0.00	0.00	26.73	41.17
	Overall Zn2p	**0.00**	**0.00**	**1023.96**	**1018.42**	**0.00**	**0.00**	**0.16**	**0.14**

Based on XPS measured atomic concentrations, it is possible to quantify the degree of the surface coverage of asphaltene on silica as follows (Wang, et al., 2013):

$$\theta = \frac{C_{coated} - C_{Si}}{C_{bulk} - C_{Si}}$$

Using the atomic ratio data from Tables 4-2 and 4-6, the following percentages of surface coverage of asphaltene can be computed:

Table 4-7. Surface Coverage of adsorbed asphaltene on silica

	Surface Coverage of asphaltene (%)	
	C1s	Si2p
Silica	0	0
Asphaltene + SiO_2	97.13	96.72
Asphaltene + ZnO	99.54	98.95
Asphaltene + NC	90.44	90.41
Asphaltene	100	100

Based on Table 4-7, it is concluded that surface coverage is the greatest in presence of ZnO nanoparticle, as it caused less changes in chemical composition of the surface compared to SiO_2. However, NC application has decreased asphaltene surface coverage by 10% which clearly demonstrates its efficiency.

Finally, by combining all data from XPS, AFM, and CA measurements, it can be concluded that ZnO-SiO_2-Thiazine nanocomposite is the most efficient asphaltene inhibitor, as it actively interacts with asphaltene molecules, thus modifying asphaltene/silica surface chemistry, which yields in the reduced amount of precipitates and the least contact angle making the surface water-wet. As far as NPs are concerned, the results of the experiments suggest ZnO to be better EOR agent compared to SiO_2, as its wettability alternating abilities are better. However, AFM and XPS results suggest SiO_2 to be better asphaltene inhibitor as it is more reactive to asphaltene.

5 Conclusions and Recommendations

Asphaltene deposition is one of the reasons of weakened oil production and deteriorated reservoir rock properties. Therefore, the evaluation of surface chemistry and morphology of the silica-asphaltene important for EOR. The primary goal of this research work was to examine the efficiency of ZnO-SiO_2-Thiazine NC and its component NPs as asphaltene inhibitors on silica surfaces using AFM, XPS, and CA measurements, which evaluated alterations in surface micro-topography, wettability, and surface chemistry for each NP and NC. A three-stage laboratory work strategy comprising NP characterization, preparation asphaltene deposited silica surfaces, and their XPS surveys, AFM and CA measurements were devised and carried out.

Asphaltene extracted from Kazakhstani crude oil was characterized using XPS and used for silica surface samples preparation. NPs and NC were then characterized by FTIR, TEM, XRD, SEM, and EDX methods to determine particle size and distribution, chemical analysis, and surface morphology. The sample surfaces were prepared based on two distinct methods for XPS and AFM. XPS, AFM, and CA measurements were taken from the following 5 surfaces: pure silica, silica + asphaltene + *n*-heptane, silica + asphaltene + *n*-heptane + ZnO, silica + asphaltene + *n*-heptane + SiO_2, and silica + asphaltene + *n*-heptane + NC. AFM was used to examine the surface topography of each silica surface sample. The CA measurements were taken to observe the wettability alteration of the samples. XPS was used to determine the elemental composition of the samples to investigate asphaltene adsorption degree.

5.1 Conclusions

Based on the findings of this research work, the following major conclusions were inferred:

1. The research of NP/NC efficiency revealed the following order from the most efficient asphaltene inhibition to the least efficient one: ZnO-SiO_2-Thiazine > SiO_2 > ZnO.
2. AFM images demonstrated asphaltene peaks in presence of NC to have the Arithmetical Mean Height of 2 times less than in NC's absence. The asphaltene peaks in presence of NC have a stretched and somewhat slanted form. Overall, the surface in presence of NC is the least rough and textured; while, presence of ZnO resulted in highest roughness.
3. NC has decreased the CA of a surface from 154.8° to 59.0°, meaning that the surface wettability altered from fully oil-wet to water-wet. On contrast, SiO_2 reduced CA of a

surface up to 115.3° and it remained oil-wet, whereas ZnO reduced CA up to 100.8° and made a surface intermediate-wet.

4. XPS results revealed that presence of NPs/NC caused chemical alterations in elemental composition of sample surfaces. Since carbon is the most prevalent element in asphaltene, it is plausible to deduce that in the presence of NP/NC, the amount of asphaltene adsorption onto the surface is reduced owing to less carbon.
5. The Surface Coverage of Asphaltene, computed based on XPS results, reduced by 10% in presence of NC, whereas ZnO and SiO_2 has decreased the surface coverage by 2-3% only.

The acquired values were achieved in the laboratory at room temperature and pressure conditions, and thus may be used as a baseline value for further studies with various chemicals and materials.

5.2 Recommendations

Further research can be conducted based on the following recommendations:

1. Further research is needed to investigate the behavior of ZnO-SiO_2-Thiazine and its NPs on silica surface under reservoir conditions. Additionally, we recommend to conduct research at various asphaltene and NP/NC concentrations to evaluate the limit of NP/NC to inhibit asphaltene in the most efficient way.

References

Abdallah, W. A. & Taylor, S. D., 2008. Study of asphaltenes adsorption on metallic surface using XPS and TOF-SIMS. *The Journal of Physical Chemistry,* 112(48), pp. 18963-18972.

Abdel-Raouf, M. E.-S., 2012. Factors Affecting the Stability of Crude Oil Emulsions. In: *Crude Oil Emulsions.* s.l.:s.n., p. 194.

Abudu, A. & Goual, L., 2009. Adsorption of Crude Oil on Surfaces Using Quartz Crystal Microbalance with Dissipation (QCM-D) under Flow Conditions. *Energy & Fuels,* 23(3), pp. 1237-1248.

Acevedo, S. et al., 1997. Observations about the Structure and Dispersion of Petroleum Asphaltenes Aggregates Obtained from Dialysis Fractionation and Characterization. *Energy & Fuels,* 11(4), pp. 774-778.

Acevedo, S., García, L. A. & Rodríguez, P., 2012. Changes in diameter distribution with temperature measured for asphaltenes and their fractions A1 and A2. Impact of measurements in colloidal and solubility issues of asphaltenes.. *Energy Fuels,* pp. 1814-1819.

Afshari, S., Kharrat, R. & Ghazanfari, M. H., 2010. *Asphaltene Precipitation Study during Natural Depletion at Reservoir Conditions.* Beijing, s.n.

Agista, M. N., Guo, K. & Yu, Z., 2018. A State-of-the-Art Review of Nanoparticles Application in Petroleum with a Focus on Enhanced Oil Recovery. *Applied Sciences,* 8(6).

Akbar, S. & Saleh, A., 1989. *A Comprehensive Approach To Solve Asphaltene Deposition Problem in Some Deep Wells.* Bahrain, s.n.

Al-Hosani, A., Ravichandran, S. & Daraboina, N., 2021. Review of Asphaltene Deposition Modeling in Oil and Gas Production. *Energy Fuels,* 35(2), pp. 965-986.

Alian, S. S., Alta'ee, A. F., Omar, A. A. & Hani, I., 2011. *Study of asphaltene precipitation during CO2 injection for Malaysian light oil reservoirs.* Perek, IEEE, pp. 1-5.

Almehaideb, R. A. & Zekri, A. Y., 2001. *Possible Use of Bacteria/Steam to Treat Asphaltene Deposition in Carbonate Rocks.* The Hague, s.n.

American Society for Testing and Material, 2013. *Standard test method for determination of asphaltenes (heptane insolubles) in crude and petroleum products ASTM international.* s.l.:Petr. Prod. Lubr. Foss. Fuels.

Andrews, A. B., Guerra, R. E., Mullins, O. C. & Sen, P. N., 2006. Diffusivity of Asphaltene Molecules by Fluorescence Correlation Spectroscopy. *The Journal of Physical Chemistry,* 110(26), pp. 8093-8097.

Bernadiner, M., 1993. *Advanced Asphaltene and Paraffin Control Technology.* New Orleans, s.n.

Bruining, I. M. d. A., Martinez, A. V. & Travalloni, A. M. L., 1990. *Identification of Asphaltene Deposition in Camorim Field, Northeastern Brazil.* Rio de Janeiro, s.n.

Buenrostro-Gonzalez, E., Groenzin, H., Lira-Galeana, C. & Mullins, O. C., 2001. The Overriding Chemical Principles that Define Asphaltenes. *Energy Fuels,* 15(4), pp. 972-978.

Dickie, J. P. & Yen, T. F., 1967. Macrostructures of the asphaltic fractions by various instrumental methods. *Analytical Chemistry,* 39(14), pp. 1847-1852.

Ekholm, P. et al., 2002. A Quartz Crystal Microbalance Study of the Adsorption of Asphaltenes and Resins onto a Hydrophilic Surface. *Journal of Colloid and Interface Science,* 247(2), pp. 342-350.

El-Sayed, M., 2012. Factors Affecting the Stability of Crude Oil Emulsions. In: *Crude Oil Emulsions- Composition Stability and Characterization.* s.l.:InTech.

Eltoum, H., Yang, Y.-L. & Hou, J.-R., 2021. The effect of nanoparticles on reservoir wettability alteration: a critical review. *Petroleum Science,* Volume 18, pp. 136-153.
Gollapudi, U., Bang, S. & Islam, M., 1994. *Ultrasonic Treatment for Removal of Asphaltene Deposits During Petroleum Production.* Lafayette, s.n.
González, M. F., Stull, C. S., López-Linares, F. & Pereira-Almao, P., 2007. Comparing Asphaltene Adsorption with Model Heavy Molecules over Macroporous Solid Surfaces. *Energy Fuels,* 21(1), pp. 234-241.
Goulon, J. et al., 1984. Structural characterization by X-ray absorption spectroscopy (EXAFS/XANES) of the vanadium chemical environment in Boscan asphaltenes. *Journal of the Chemical Society, Dalton Transactions,* Issue 6, pp. 1095-1103.
Groenzin, H. & Mullins, O. C., 1999. Asphaltene Molecular Size and Structure. *The Journal of Physical Chemistry,* 103(50), pp. 11237-11245.
Groenzin, H. & Mullins, O. C., 2000. Molecular Size and Structure of Asphaltenes from Various Sources. *Energy Fuels,* 14(3), pp. 677-684.
Hasanvand, M. Z. et al., 2018. A literature review of asphaltene entity, precipitation, and deposition: introducing recent models of deposition in the well column. *Journal of Oil, Gas and Petrochemical Sciences,* 1(3), pp. 83-89.
Hendraningrat, L., Li, S. & Torsaeter, O., 2013. *Enhancing Oil Recovery of Low-Permeability Berea Sandstone through Optimized Nanofluids Concentration.* Kuala Lumpur, s.n.
Hirschberg, A., deJong, L. N. J., Schipper, B. A. & Meijer, J. G., 1984. Influence of Temperature and Pressure on Asphaltene Flocculation. *SPE Journal,* 24(3), pp. 283-293.
Hoepfner, M. P. et al., 2013. A Fundamental Study of Asphaltene Deposition. *Energy Fuels,* 27(2), pp. 725-735.
Hu, C. et al., 2015. Role of Water on the Precipitation and Deposition of Asphaltenes in Packed-Bed Microreactors. *Industrial and Engineering Chemistry Research,* 54(16), pp. 4103-4112.
Jada, A. & Debih, H., 2009. Hydrophobation of Clay Particles by Asphaltenes Adsorption. *Composite Interfaces,* 16(2-3), pp. 219-235.
Karimi, A. et al., 2011. Quantitative Evidence for Bridged Structures in Asphaltenes by Thin Film Pyrolysis. *Energy Fuels,* 25(8), pp. 3581-3589.
Kaveh, N. S. et al., 2014. Wettability Evaluation of a CO2/Water/Bentheimer Sandstone System: Contact Angle, Dissolution, and Bubble Size. *Energy Fuels,* 28(6), pp. 4002-4020.
Kaveh, N. S. et al., 2014. Wettability Evaluation of a CO2/Water/Bentheimer Sandstone System: Contact Angle, Dissolution, and Bubble Size. *Energy Fuels,* 28(6), pp. 4002-4020.
Keshavarz, B., Dehaghani, A. H. S. & Dehghani, S. A. M., 2019. Investigation the impact of additives on the displacement of the onset point of asphaltene precipitation using interfacial tension measurement. *Energy Sources, Part A: Recovery, Utilization, and Environmental Effects,* 41(11), pp. 1360-1371.
Kokal, S. L. & Sayegh, S. G., 1995. *Asphaltenes: The Cholesterol Of Petroleum.* Bahrain, s.n.
Kumar, G., Behera, U. S., Mani, E. & Sangwai, J. S., 2022. Engineering the Wettability Alteration of Sandstone Using Surfactant-Assisted Functional Silica Nanofluids in Low-Salinity Seawater for Enhanced Oil Recovery. *ACS Engineering,* 2(5), pp. 421-435.
Kumar, K., Dao, E. & Mohanty, K., 2004. AFM study of mineral wettability with reservoir oils. *Journal of Colloid and Interface Science,* 247(2), pp. 342-350.
León, O. et al., 2002. Adsorption of Native Resins on Asphaltene Particles: A Correlation between Adsorption and Activity. *Langmuir,* 18(13), pp. 5106-5112.

Li, S. et al., 2021. Visualizing and Quantifying Wettability Alteration by Silica Nanofluids. *Applied Materials and Interfaces,* 13(34), pp. 41182-41189.
López-Linares, F. et al., 2006. Quinolin-65 and Violanthrone-79 as Model Molecules for the Kinetics of the Adsorption of C7 Athabasca Asphaltene on Macroporous Solid Surfaces. *Energy Fuels,* 20(6), pp. 2748-2750.
Medina, O. et al., 2019. Nanotechnology Applied to Thermal Enhanced Oil Recovery Processes: A Review.. *Energies,* 12(24).
Mohammadi, M. et al., 2011. Inhibition of Asphaltene Precipitation by TiO2, SiO2, and ZrO2 Nanofluids. *Energy Fuels,* 25(7), pp. 3150-3156.
Mohammadi, M., Mousavi-Dehghani, S. A. & Ameri, M. J., 2012. *Experimental investigation of asphaltene adsorption on different mineral surfaces and effect of various parameters on the adsorption rate: Study of adsorption with UV spectroscopy.* San Diego, s.n.
Mohammed, I. et al., 2021. Impact of Asphaltene Precipitation and Deposition on Wettability and Permeability. *ACS Omega,* 6(31), pp. 20091-20102.
Mohammed, M. & Babadagli, T., 2015. Wettability alteration: A comprehensive review of materials/methods and testing the selected ones on heavy-oil containing oil-wet systems. *Advances in Colloid and Interface Science,* Volume 220, pp. 54-77.
Morante, L. R., Poveda, J.-. C., Campos, R. M.-. & Martínez, J. A. H.-., 2017. Aggregate structure analysis of Colombian heavy crude oil-derived asphaltenes using small angle X-ray scattering. *CT&F - Ciencia, Tecnología & Futuro,* 6(5).
Mullins, O. C., 2010. The Modified Yen Model. *Energy Fuels,* 24(4), pp. 2179-2207.
Nakajima, A., 2011. Design of hydrophobic surfaces for liquid droplet control. *NPG Asia Materials,* Volume 3, pp. 49-56.
Nassar, N. N., Hassan, A. & Pereira-Almao, P., 2011. Metal Oxide Nanoparticles for Asphaltene Adsorption and Oxidation. *Energy Fuels,* 25(3), pp. 1017-1023.
Pierre, C., Barré, L., Pina, A. & Moan, M., 2004. Composition and Heavy Oil Rheology. *Oil & Gas Science and Technology,* 59(5), pp. 489-501.
Podgorski, D. C. et al., 2013. Heavy Petroleum Composition. 5. Compositional and Structural Continuum of Petroleum Revealed. *Energy Fuels,* 27(3), pp. 1268-1276.
Poveda, J. C. et al., 2014. Molecular Changes in Asphaltenes within H2 Plasma. *Energy Fuels,* 28(2), pp. 735-744.
Ramos, A. C. d. S. et al., 2001. Interfacial and colloidal behavior of asphaltenes obtained from Brazilian crude oils. *Journal of Petroleum Science and Engineering,* 32(2-4), pp. 201-216.
Rodgers, R. & Marshall, A., 2007. Petroleomics: Advanced Characterization of Petroleum-Derived Materials by Fourier Transform Ion Cyclotron Resonance Mass Spectrometry (FT-ICR MS). In: *Asphaltenes, Heavy Oils, and Petroleomics.* New York: Springer, pp. 69-93.
Rueda-Velasquez, R. I. et al., 2013. Characterization of Asphaltene Building Blocks by Cracking under Favorable Hydrogenation Conditions. *Energy Fuels,* 27(4), pp. 1817-1829.
Sarma, H. K., 2003. *Can We Ignore Asphaltene in a Gas Injection Project for Light-Oils?.* Kuala Lumpur, s.n.
Schuler, B. et al., 2015. Unraveling the Molecular Structures of Asphaltenes by Atomic Force Microscopy. *Journal of the American Chemical Society,* 137(31), pp. 9870-9876.
Seifert, D. J. et al., 2012. *Black Oil, Heavy Oil and Tar in One Oil Column Understood by Simple Asphaltene Nanoscience.* Abu Dhabi, s.n.

Seyyedi, M., Sohrabi, M. & Farzaneh, A., 2015. *Investigation of Rock Wettability Alteration by Carbonated Water - Contact Angle Measurement.* s.l., European Association of Geoscientists & Engineers.
Sheremata, J. M., Gray, M. R., Dettman, H. D. & McCaffrey, W. C., 2004. Quantitative Molecular Representation and Sequential Optimization of Athabasca Asphaltenes. *Energy Fuels,* 18(5), pp. 1377-1384.
Shojaati, F., Riazi, M., Mousavi, S. H. & Derikvand, Z., 2017. Experimental investigation of the inhibitory behavior of metal oxides nanoparticles on asphaltene precipitation. *Colloids and Surfaces A: Physicochemical and Engineering Aspects,* Volume 531, pp. 99-110.
Si, J., Li, X.-C. & Cui, B.-K., 2014. Decolorization of heterocycle dye Neutral Red by white-rot fungus Perenniporia subacida. *Desalination and Water Treatment,* pp. 5594-5604.
Strausz, O. P., Mojelsky, T. W. & Lown, E. M., 1992. The molecular structure of asphaltene: an unfolding story. *Fuel,* 71(12), pp. 1355-1363.
Sun, X., Zhang, Y., Chen, G. & Gai, Z., 2017. Application of Nanoparticles in Enhanced Oil Recovery: A Critical Review of Recent Progress. *Energies,* 10(3), p. 345.
Tajmiri, M. et al., 2015. Wettability Alteration of Sandstone and Carbonate Rocks by Using ZnO Nanoparticles in Heavy Oil Reservoirs. *Iranian Journal of Oil and Gas Science and Technology,* 4(4), pp. 50-66.
Tazikeh, S. et al., 2020. Bi-fractal and bi-Gaussian theories to evaluate impact of polythiophene-coated Fe3O4 nanoparticles on asphaltene precipitation and surface topography. *Fuel,* Volume 272, p. 117535.
Tazikeh, S., Amin, J. S., Zendehboudi, S. & Shafiei, A., 2022. Effects of asphaltene structure and polythiophene-coated magnetite nanoparticles on surface topography and wettability alteration of silica surface. *Journal of Molecular Liquids,* Volume 349, p. 118470.
Tazikeh, S. et al., 2021. Molecular dynamics simulation to investigate the effect of polythiophene-coated Fe3O4 nanoparticles on asphaltene precipitation. *Chemical Engineering Science,* Volume 237, p. 116417.
Vargas, F. M., Gonzalez, D. L., Hirasaki, G. J. & Chapman, W. G., 2009. Modeling Asphaltene Phase Behavior in Crude Oil Systems Using the Perturbed Chain Form of the Statistical Associating Fluid Theory (PC-SAFT) Equation of State. *Energy Fuels,* 23(3), pp. 1140-1146.
Vargas, F. M. & Tavakkoli, M., 2018. *Asphaltene Deposition: Fundamentals, Prediction, Prevention, and Remediation.* s.l.:CRC Press.
Wang, S. et al., 2013. Study of Asphaltene Adsorption on Kaolinite by X-ray Photoelectron Spectroscopy and Time-of-Flight Secondary Ion Mass Spectroscopy. *Energy Fuels,* Volume 27, pp. 2465-2473.
Wang, S. et al., 2016. Adsorption of asphaltenes on kaolinite as an irreversible process. *Colloids and Surfaces A: Physicochemical and Engineering Aspects,* Volume 504, pp. 280-286.
Wiehe, I. A., 2012. Asphaltene Solubility and Fluid Compatibility. *Energy Fuels,* 26(7), pp. 4004-4016.
Zendehboudi, S., 2019. Chapter 3 | Asphaltenes Review: Characterization and Modeling. In: *Fuels and Lubricants Handbook: Technology, Properties, Performance, and Testing.* 2nd ed. s.l.:ASTM International, pp. 39-77.